ELSEVIER

Comput. Methods Appl. Mech. Engrg. 190 (2001) 2555–2580

Computer methods in applied mechanics and engineering

www.elsevier.com/locate/cma

Strain localization in frictional materials exhibiting displacement jumps

Ronaldo I. Borja *, Richard A. Regueiro

Department of Civil and Environmental Engineering, Stanford University, Stanford, CA 94305-4020, USA

Received 12 January 1998; received in revised form 11 January 2000

Abstract

This paper presents a mathematical model for analyzing strain localization in frictional solids exhibiting displacement jumps. Precise conditions for the appearance of slip lines, including their initiation and evolution, are outlined for a rate-independent, strain-softening Drucker–Prager model, and explicit analytical expressions are used to describe the orientation of the slip line. A stress–displacement relation obtained through the consistency condition is also formulated to describe the quasi-static response in the post-localization regime. The mathematical model, which is cast within the framework of finite element analysis employing the assumed enhanced strain method, circumvents mesh-dependence issues often associated with rate-independent plasticity models. It is shown that the enhancement equation is nothing else but the consistency condition imposed on the band. Numerical examples involving plane strain compression are described to demonstrate objectivity with respect to mesh refinement and insensitivity to mesh alignment of finite element solutions.

1. Introduction

Many problems in geomechanics require a mathematical description of failure and post-failure conditions of geotechnical structures such as dams, embankments, excavations, foundations, and slopes. Failures of these structures are often accompanied by the appearance of highly localized patterns of deformation, ultimately leading to the development of a well-defined failure mechanism. The failure mechanism manifests in the form of a slip surface along which relatively rigid masses of earth slide past each other. The band of intense shearing has an initial characteristic width or thickness, but this thickness could shrink to zero as the slip surface develops completely. Mathematically, the continuum experiences displacement jumps along this slip surface.

The limit equilibrium method is commonly used to examine the failure mechanism of geotechnical structures. Examples of the limit equilibrium method for geotechnical analyses are the Coulomb, trial wedge, and slip circle methods, as well as a large family of slope stability analysis methods. The limit equilibrium method requires that the surface of discontinuity be defined a priori, and does not describe patterns of deformation in the continuum. In particular, the method does not account for the softening response along the surface of discontinuity, and hence, it is useful only for stability analysis but not for deformation analysis.

The standard finite element method has been used successfully to solve a wide variety of deformation-type continuum problems, but its application to analysis of failure and post-failure conditions is severely limited by its inability to resolve the effect of strain localization along a narrow shear band. This

* Corresponding author.

0045-7825/01/$ - see front matter
PII: S0045-7825(00)00253-X

shortcoming is due to the general requirement that the standard finite elements be conforming, which renders the acceptability of the method dependent on how accurately the finite element mesh can resolve the strain localization across the thickness of the shear band. The difficulty is compounded further by the fact that rate-independent plasticity models do not provide a characteristic length scale that fixes the thickness of the shear band.

The assumption that the band thickness is zero creates a scenario in which the constitutive model is not required to provide a characteristic length scale. However, this assumption is tantamount to allowing the development of jumps or discontinuities in the displacement field. Mathematically, the strains or deformations generated by this displacement field are δ-functions along the surface of discontinuity, and so plastic deformations can be assumed to be localized to this discontinuity. The problem of strain localization involving displacement jumps has been termed "strong discontinuity" in [1], in contrast to the problem involving strain or deformation jumps, which has been termed "weak discontinuity" also in [1].

The assumption of a zero band thickness is a mathematical simplification since it avoids the problem associated with the lack of a characteristic length scale in rate-independent solids, but it has some strong physical justifications for geologic media. Soils and rocks routinely exhibit cracking and faulting when sheared [2], leading to jumps in the displacement field. Even clays subjected to plastic flow can undergo sliding and splitting [3]. Further, the thickness of shear band in sands can vary between 10 and 20 times the mean grain size diameter [4,5], which is small compared to typical dimensions of geotechnical structures. The assumption of displacement jumps was central to the development of Coulomb's [6] and Rankine's [7] methods of earth pressure calculations, to Terzaghi's [8] and Meyerhof's [9] methods of bearing capacity analyses, and to many slope stability analysis methods [10,11]. In contrast, shear bands observed in a variety of metals are of finite thickness, such as those first identified as the so-called heat lines in the experimental work of Tresca (see [12]), so that jumps in displacements in this material may not be fully realized.

Finite element analyses of strain localization in solids exhibiting displacement jumps have been presented recently in [1,13–18] within the context of strain-softening, J_2 flow theory and a damage model. Precise conditions for the appearance of slip lines have been outlined for rate-independent problems in the quasi-static regime, and finite element approximations for the post-localization regime have been formulated within the context of the assumed enhanced strain methods described in [19]. It has now been demonstrated that the strong discontinuity approach coupled with the assumed enhanced strain method could circumvent mesh-dependence issues often associated with rate-independent plasticity models [20,21]. Furthermore, the approach does not require any viscoplastic regularization [22,23] or more complicated reformulations of the constitutive equation [24,25] to advance the solution to the post-bifurcation regime. The objective of this paper is to exploit these important features for the analysis of strain localization in frictional materials exhibiting displacement jumps. To this end, we consider a two-invariant, non-associated Drucker–Prager plasticity model and outline precise conditions for the appearance of slip lines in this material.

The Drucker–Prager model allows the analysis of several relevant features not captured by the J_2 plasticity model, such as the influence of the mean normal stress on yielding, the effect of plastic dilatation along the slip line, and the general treatment of plasticity models with non-associated plastic flow. The choice of this specific plasticity model is motivated by its capability to describe the behavior of dilatant frictional materials. In addition to defining conditions for the appearance of slip lines, this paper also covers the general stress–displacement relationship at post-localization on frictional materials.

As for notations and symbols, bold-face letters denote matrices and vectors; the symbol '$\cdot$' denotes an inner product of two vectors (e.g. $\boldsymbol{a} \cdot \boldsymbol{b} = a_i b_i$), or a single contraction of adjacent indices of two tensors (e.g. $\boldsymbol{c} \cdot \boldsymbol{d} = c_{ij} d_{jk}$); the symbol ':' denotes an inner product of two second-order tensors (e.g. $\boldsymbol{c} : \boldsymbol{d} = c_{ij} d_{ij}$), or a double contraction of adjacent indices of tensors of rank two and higher (e.g. $\boldsymbol{C} : \boldsymbol{\epsilon}^{\mathrm{e}} = C_{ijkl} \epsilon^{\mathrm{e}}_{kl}$).

2. Model problem for non-associated plasticity

In order to study the important features of solutions involving jumps in displacement field in dilatant frictional materials, we consider the general case of non-associated rate-independent plasticity in the classical format of infinitesimal strains for an intact continuum. We next investigate conditions for the

onset of displacement jumps in the continuum. Subsequently, we introduce a damage function, which may be distinct from the yield function, to characterize the response of the material in the bifurcated stage. In the next section, we specialize the formulation to non-associated Drucker–Prager plasticity and accommodate the presence of displacement jumps in this material.

2.1. Infinitesimal plasticity theory for intact continuum

Consider a convex elastic domain $\boldsymbol{E}$ defined by a smooth yield surfact $\mathscr{F}$ in the Cauchy stress space $\boldsymbol{\sigma}$

$$\boldsymbol{E} = \{(\boldsymbol{\sigma}, \boldsymbol{\theta}) \in S \times \mathbb{R}^m \,|\, \mathscr{F}(\boldsymbol{\sigma}, \boldsymbol{\theta}) \leqslant 0\}, \tag{2.1}$$

where S is the space of symmetric rank-two tensors and $\boldsymbol{\theta}$ is a stress-like vector of plastic internal variables of dimension m characterizing the hardening response of the material. The constitutive equation is expressed in terms of a free energy function $\Psi(\boldsymbol{\epsilon}^{\mathrm{e}}, \boldsymbol{\xi})$, where $\boldsymbol{\epsilon}^{\mathrm{e}}$ is the elastic component of the infinitesimal strain tensor, and $\boldsymbol{\xi}$ denotes a strain-like vector of plastic variables conjugate to $\boldsymbol{\theta}$. By definition, the constitutive equations for $\boldsymbol{\sigma}$ and $\boldsymbol{\theta}$ take the form

$$\boldsymbol{\sigma} = \frac{\partial \Psi(\boldsymbol{\epsilon}^{\mathrm{e}}, \boldsymbol{\xi})}{\partial \boldsymbol{\epsilon}^{\mathrm{e}}}, \quad \boldsymbol{\theta} = -\frac{\partial \Psi(\boldsymbol{\epsilon}^{\mathrm{e}}, \boldsymbol{\xi})}{\partial \boldsymbol{\xi}}. \tag{2.2}$$

We next consider a plastic potential function $\mathscr{Q}(\boldsymbol{\sigma}, \boldsymbol{\theta})$, which can be distinct from $\mathscr{F}(\boldsymbol{\sigma}, \boldsymbol{\theta})$. The special case $\partial\mathscr{Q}/\partial\boldsymbol{\sigma} = \partial\mathscr{F}/\partial\boldsymbol{\sigma}$ pertains to associative plasticity, while the case $\partial\mathscr{Q}/\partial\boldsymbol{\theta} = \partial\mathscr{F}/\partial\boldsymbol{\theta}$ corresponds to associative hardening. Let the total infinitesimal strain tensor be decomposed into elastic and plastic parts, i.e. $\boldsymbol{\epsilon} = \boldsymbol{\epsilon}^{\mathrm{e}} + \boldsymbol{\epsilon}^{\mathrm{p}}$. Then the evolution equations for $\boldsymbol{\epsilon}^{\mathrm{e}}$ and $\boldsymbol{\xi}$ take the form

$$\dot{\boldsymbol{\epsilon}}^{\mathrm{e}} = \dot{\boldsymbol{\epsilon}} - \lambda \frac{\partial \mathscr{Q}(\boldsymbol{\sigma}, \boldsymbol{\theta})}{\partial \boldsymbol{\sigma}}, \quad \dot{\boldsymbol{\xi}} = \lambda \frac{\partial \mathscr{Q}(\boldsymbol{\sigma}, \boldsymbol{\theta})}{\partial \boldsymbol{\theta}}, \tag{2.3}$$

where λ is a plastic consistency parameter satisfying the Kuhn–Tucker complementary conditions

$$\lambda \geqslant 0, \quad \mathscr{F}(\boldsymbol{\sigma}, \boldsymbol{\theta}) \leqslant 0, \quad \lambda \mathscr{F}(\boldsymbol{\sigma}, \boldsymbol{\theta}) = 0. \tag{2.4}$$

The general setting is provided by the continuum model described above. We will now provide extension of the model to include the presence of a discontinuous displacement field.

2.2. Constitutive theory in the presence of discontinuous displacement field

Consider the following displacement field with a jump discontinuity:

$$\boldsymbol{u} = \overline{\boldsymbol{u}} + [\![\boldsymbol{u}]\!] H_{\mathscr{S}}(\boldsymbol{x}), \quad H_{\mathscr{S}}(\boldsymbol{x}) = \begin{cases} 1 & \text{if } \boldsymbol{x} \in \Omega_+, \\ 0 & \text{if } \boldsymbol{x} \in \Omega_-, \end{cases} \tag{2.5}$$

where $\overline{\boldsymbol{u}}$ is the continuous part of $\boldsymbol{u}$, and $[\![\boldsymbol{u}]\!]$ is the jump discontinuity on the surface $\mathscr{S}$ separating the subdomains Ω_+ and Ω_- of an otherwise continuous body Ω. The associated total strain rate tensor resulting from this field is the symmetric component of the displacement gradient tensor, which can be written in compact form as [1]

$$\dot{\boldsymbol{\epsilon}} = \mathrm{sym}(\nabla \dot{\overline{\boldsymbol{u}}}) + \mathrm{sym}([\![\dot{\boldsymbol{u}}]\!] \otimes \boldsymbol{n} \delta_{\mathscr{S}}), \tag{2.6}$$

where $\boldsymbol{n}$ is the unit normal vector to the surface $\mathscr{S}$ and pointing in the direction of Ω_+, and $\delta_{\mathscr{S}}$ is the Dirac delta function on the surface $\mathscr{S}$.

Since $\mathscr{F}(\boldsymbol{\sigma}, \boldsymbol{\theta}) = 0$ on initial yielding, and remains equal to zero during yielding, we obtain the consistency condition

$$\dot{\mathscr{F}}(\boldsymbol{\sigma}, \boldsymbol{\theta}) = \frac{\partial \mathscr{F}}{\partial \boldsymbol{\sigma}} : \boldsymbol{C} : \left[\mathrm{sym}(\nabla \dot{\overline{\boldsymbol{u}}}) + \mathrm{sym}([\![\dot{\boldsymbol{u}}]\!] \otimes \boldsymbol{n} \delta_{\mathscr{S}}) - \lambda \frac{\partial \mathscr{Q}}{\partial \boldsymbol{\sigma}} \right] - \lambda \frac{\partial \mathscr{F}}{\partial \boldsymbol{\theta}} \cdot \boldsymbol{H} \cdot \frac{\partial \mathscr{Q}}{\partial \boldsymbol{\theta}} = 0, \tag{2.7}$$

where

$$\boldsymbol{C} = \frac{\partial^2 \Psi(\boldsymbol{\epsilon}^{\mathrm{e}}, \boldsymbol{\xi})}{\partial \boldsymbol{\epsilon}^{\mathrm{e}} \partial \boldsymbol{\epsilon}^{\mathrm{e}}}, \quad \boldsymbol{H} = \frac{\partial^2 \Psi(\boldsymbol{\epsilon}^{\mathrm{e}}, \boldsymbol{\xi})}{\partial \boldsymbol{\xi} \partial \boldsymbol{\xi}} \tag{2.8}$$

are the (symmetric) Hessian tensors of $\Psi(\boldsymbol{\epsilon}^{\mathrm{e}}, \boldsymbol{\xi})$ evaluated with respect to $\boldsymbol{\epsilon}^{\mathrm{e}}$ and $\boldsymbol{\xi}$, respectively. The tensors $\boldsymbol{C}$ and $\boldsymbol{H}$ have the physical significance of being the tangential elastic stress–strain tensor and the tangential plastic moduli matrix, respectively.

Hardening, softening, or perfect plasticity is determined by whether the following parameter is greater than, less than, or equal to zero

$$\mathscr{H} := \frac{\partial \mathscr{F}}{\partial \boldsymbol{\theta}} \cdot \boldsymbol{H} \cdot \frac{\partial \mathscr{Q}}{\partial \boldsymbol{\theta}}. \tag{2.9}$$

Although softening response could entail the development of solutions exhibiting displacement jumps [26,27], we will not rule out the case of hardening response. Satisfaction of (2.7) for non-trivial value of $[\![\dot{\boldsymbol{u}}]\!]$ requires that λ and $\mathscr{H}$ be of the form [1]

$$\lambda = \lambda_\delta \delta_{\mathscr{S}}, \quad \mathscr{H}^{-1} = \mathscr{H}_\delta^{-1} \delta_{\mathscr{S}}, \tag{2.10}$$

where $\lambda_\delta > 0$ and $\mathscr{H}_\delta < 0$ are real, non-singular functions. The setting described by (2.10) thus requires that λ and $\mathscr{H}$ be treated as distribution functions.

With (2.10) in hand, it is now possible to impose the consistency condition (2.7). Setting the regular and singular parts to zero, we obtain the two separate conditions

$$\frac{\partial \mathscr{F}}{\partial \boldsymbol{\sigma}} : \boldsymbol{C} : \mathrm{sym}(\nabla \dot{\boldsymbol{u}}) - \lambda_\delta \mathscr{H}_\delta = 0 \tag{2.11}$$

for the regular part, and

$$\frac{\partial \mathscr{F}}{\partial \boldsymbol{\sigma}} : \boldsymbol{C} : \left[\mathrm{sym}([\![\dot{\boldsymbol{u}}]\!] \otimes \boldsymbol{n}) - \lambda_\delta \frac{\partial \mathscr{Q}}{\partial \boldsymbol{\sigma}} \right] = 0 \tag{2.12}$$

for the singular part. Solving (2.12) for λ_δ gives

$$\lambda_\delta = \frac{1}{\chi} \frac{\partial \mathscr{F}}{\partial \boldsymbol{\sigma}} : \boldsymbol{C} : \mathrm{sym}([\![\dot{\boldsymbol{u}}]\!] \otimes \boldsymbol{n}), \quad \chi = \frac{\partial \mathscr{F}}{\partial \boldsymbol{\sigma}} : \boldsymbol{C} : \frac{\partial \mathscr{Q}}{\partial \boldsymbol{\sigma}}. \tag{2.13}$$

Since $\lambda_\delta \mathscr{H}_\delta < 0$, by definition, then (2.11) implies that $\partial \mathscr{F} / \partial \boldsymbol{\sigma} : \boldsymbol{C} : \mathrm{sym}(\nabla \dot{\boldsymbol{u}}) < 0$, and so at the instant of localization the stress point *unloads elastically* as a continuum relative to the current value of $\mathscr{F}$, with $\dot{\boldsymbol{\sigma}} = \boldsymbol{C} : \mathrm{sym}(\nabla \dot{\boldsymbol{u}})$ representing the continuum stress rate.

2.3. Localization condition

Equilibrium requires continuity of the traction vector $\boldsymbol{t}$ (as well as its rate, $\dot{\boldsymbol{t}}$) across $\mathscr{S}$. For the model problem, we have

$$\dot{\boldsymbol{t}} = \boldsymbol{n} \cdot \dot{\boldsymbol{\sigma}} = \boldsymbol{n} \cdot \boldsymbol{C} : \left(\dot{\boldsymbol{\epsilon}} - \lambda \frac{\partial \mathscr{Q}}{\partial \boldsymbol{\sigma}} \right) = \dot{\bar{\boldsymbol{t}}} + \dot{\boldsymbol{t}}_\delta \delta_{\mathscr{S}}, \tag{2.14}$$

where

$$\dot{\bar{\boldsymbol{t}}} = \boldsymbol{n} \cdot \boldsymbol{C} : \mathrm{sym}(\nabla \dot{\boldsymbol{u}}) \tag{2.15}$$

is the regular part, and

$$\dot{\boldsymbol{t}}_\delta = \boldsymbol{n} \cdot \boldsymbol{C}^{\mathrm{ep}} : \mathrm{sym}([\![\dot{\boldsymbol{u}}]\!] \otimes \boldsymbol{n}) \tag{2.16}$$

is the singular part, with

$$\boldsymbol{C}^{\mathrm{ep}} = \boldsymbol{C} - \boldsymbol{C}^{\mathrm{p}}, \quad \boldsymbol{C}^{\mathrm{p}} := \frac{1}{\chi}\boldsymbol{C} : \frac{\partial \mathscr{Q}}{\partial \boldsymbol{\sigma}} \otimes \frac{\partial \mathscr{F}}{\partial \boldsymbol{\sigma}} : \boldsymbol{C} \tag{2.17}$$

representing the *elastic-perfectly plastic* tangent operator. The tensor $\boldsymbol{C}^{\mathrm{ep}}$ has a structure that is mathematically similar to the continuum elasto-plastic tangent operator $\boldsymbol{c}^{\mathrm{ep}}$ used in classical plasticity theory, except that the former is defined with the denominator χ devoid of the hardening parameter. This is due to the assumption that $\mathscr{H}^{-1}$ only contains a delta-term, which effectively limits the plastic response to the band.

Let the strength, or magnitude, of the jump rate $[\![\dot{\boldsymbol{u}}]\!]$ be denoted by $\dot{\zeta}$, and let $\boldsymbol{m}$ represent a unit vector describing its direction such that $[\![\dot{\boldsymbol{u}}]\!] = \dot{\zeta}\boldsymbol{m}$. Using these definitions, and setting $\dot{\boldsymbol{t}}_\delta = 0$ in (2.16), we obtain the localization condition

$$\boldsymbol{A} \cdot \boldsymbol{m} = 0, \quad \boldsymbol{A} = \boldsymbol{n} \cdot \boldsymbol{C}^{\mathrm{ep}} \cdot \boldsymbol{n}, \tag{2.18}$$

where $\boldsymbol{A}$ is the elastic-perfectly plastic acoustic tensor. It is again noted that the tensor $\boldsymbol{A}$ has a structure that is mathematically similar to that of the elastoplastic acoustic tensor used in classical weak discontinuity-type formulations, except that the expression for the former does not contain the hardening parameter $\mathscr{H}$.

Non-trivial solutions of (2.18) are, of course, possible only when $\boldsymbol{A}$ is singular. This happens initially when the determinant of $\boldsymbol{A}$ becomes equal to zero. If the determinant indeed becomes equal to zero, it will approach this value from the positive side, since

$$\boldsymbol{A} = \boldsymbol{n} \cdot (\boldsymbol{C} - \boldsymbol{C}^{\mathrm{p}}) \cdot \boldsymbol{n} = \boldsymbol{A}^{\mathrm{e}} - \boldsymbol{A}^{\mathrm{p}} \tag{2.19}$$

and $\det(\boldsymbol{A}^{\mathrm{e}}) > 0$ since $\boldsymbol{C}$ is positive definite. For the plane strain case, the solution of (2.18) can be obtained either numerically (e.g., using the algorithm of [20,21]), or in closed form. For the non-associated Drucker–Prager plasticity model, the closed form solution for the vanishing of the determinant of $\boldsymbol{A}$ in plane strain is provided in the next section.

Remark 1. If the tensor $\mathrm{sym}([\![\dot{\boldsymbol{u}}]\!] \otimes \boldsymbol{n})$ is assumed to take the form

$$\mathrm{sym}([\![\dot{\boldsymbol{u}}]\!] \otimes \boldsymbol{n}) = \lambda \frac{\partial \mathscr{Q}}{\partial \boldsymbol{\sigma}}, \tag{2.20}$$

where λ is a proportionality coefficient, then a direct substitution of (2.20) into (2.16) automatically results in the localization condition $\dot{\boldsymbol{t}}_\delta = \boldsymbol{0}$. This is true because $\partial \mathscr{Q}/\partial \boldsymbol{\sigma}$ belongs in the nullspace of $\boldsymbol{C}^{\mathrm{ep}}$ [28], and so any tensor of the form (2.20) satisfies the homogeneous equation (2.18). This argument is central to the development of [13,14], which, unfortunately, is incorrect for the general 3D case (except for the very special case of plane strain with J_2 plastic flow) since $\partial \mathscr{Q}/\partial \boldsymbol{\sigma}$ is not an acceptable form for $\mathrm{sym}([\![\dot{\boldsymbol{u}}]\!] \otimes \boldsymbol{n})$: the latter tensor is derived from the dyad of two vectors, $[\![\dot{\boldsymbol{u}}]\!]$ and $\boldsymbol{n}$, and therefore can have at the most only two non-zero eigenvalues, whereas the tensor $\partial \mathscr{Q}/\partial \boldsymbol{\sigma}$ generally has three non-zero eigenvalues even for the simple case of J_2 plastic flow. This issue is elaborated further in Remark 3 given later in this section.

2.4. Evolution of displacement jump: damage model

Eq. (2.18) defines a necessary condition for the onset of displacement jumps. A central assumption that led to this condition was that plasticity is localized to the discontinuity, and so any point in the neighborhood of the surface of discontinuity effectively unloads once the surface of discontinuity, or band, has formed. It is therefore important to distinguish between the response of the intact continuum and the bifurcated response of the damaged material, since the former response represents the behavior of the continuum outside the band, whereas the latter response represents the behavior of a macroscopic point on the band. In particular, we elaborate the dual nature of the response of a macroscopic point in the neighborhood of the surface of discontinuity according to whether this point is interpreted to be on the band, or just outside the band. First, we introduce a model characterizing the bifurcated response, herein called the damage model.

Consider a convex elastic domain $\boldsymbol{E}'$ defined by a smooth damage function $\mathscr{G}$ in the Cauchy stress space $\boldsymbol{\sigma}$

$$\boldsymbol{E}' = \{(\boldsymbol{\sigma}, \boldsymbol{\phi}) \in S \times \mathbb{R}^n | \mathscr{G}(\boldsymbol{\sigma}, \boldsymbol{\phi}) \leqslant 0\}, \tag{2.21}$$

where S is the space of symmetric rank-two tensors, and $\boldsymbol{\phi}$ is another stress-like vector of plastic internal variables of dimension n characterizing the *softening* response of a damaged material. The damage function $\mathscr{G}$ is introduced in addition to the yield function $\mathscr{F}$ in order to differentiate between the constitutive response of the material in the intact state and its response in the damaged state. In addition, we consider a damage potential function $\mathscr{R}$, which takes on a parallel definition to the plastic potential $\mathscr{Q}$, describing the irreversible deformation response of the material in the damaged state.

Yielding in the damaged state is described by the consistency condition

$$\dot{\mathscr{G}}(\boldsymbol{\sigma}, \boldsymbol{\phi}) = \frac{\partial \mathscr{G}}{\partial \boldsymbol{\sigma}} : \boldsymbol{C} : \left[\operatorname{sym}(\nabla \dot{\overline{\boldsymbol{u}}}) + \operatorname{sym}(\llbracket \dot{\boldsymbol{u}} \rrbracket \otimes \boldsymbol{n} \delta_{\mathscr{S}}) - \lambda \frac{\partial \mathscr{R}}{\partial \boldsymbol{\sigma}} \right] - \lambda \overline{\mathscr{H}} = 0, \tag{2.22}$$

where $\overline{\mathscr{H}}$ is the softening modulus in the damaged state which takes on a parallel definition to the parameter $\mathscr{H}$ in the intact state. Assuming that plasticity remains localized to the discontinuity, then the distribution function (2.10) remain valid, and so the consistency condition (2.22) implies the two separate conditions

$$\frac{\partial \mathscr{G}}{\partial \boldsymbol{\sigma}} : \boldsymbol{C} : \operatorname{sym}(\nabla \dot{\overline{\boldsymbol{u}}}) - \lambda_\delta \mathscr{H}_\delta = 0 \tag{2.23}$$

for the regular part, and

$$\frac{\partial \mathscr{G}}{\partial \boldsymbol{\sigma}} : \boldsymbol{C} : \left[\operatorname{sym}(\llbracket \dot{\boldsymbol{u}} \rrbracket \otimes \boldsymbol{n}) - \lambda_\delta \frac{\partial \mathscr{R}}{\partial \boldsymbol{\sigma}} \right] = 0 \tag{2.24}$$

for the singular part. Since $\lambda_\delta \mathscr{H}_\delta < 0$, by definition, then (2.23) implies that $\partial \mathscr{G} / \partial \boldsymbol{\sigma} : \boldsymbol{C} : \operatorname{sym}(\nabla \dot{\overline{\boldsymbol{u}}}) < 0$, effectively capturing the softening response, with $\dot{\boldsymbol{\sigma}} = \boldsymbol{C} : \operatorname{sym}(\nabla \dot{\overline{\boldsymbol{u}}})$ representing the continuum stress rate. Condition (2.23) thus requires that the stress point remain on $\mathscr{G}$ as the size of the damage function shrinks at a rate of $\lambda_\delta \mathscr{H}_\delta$.

Eq. (2.24) restricts the magnitude and direction of the slip rate according to the damage potential function $\mathscr{R}$. Solving (2.24) for λ_δ gives

$$\lambda_\delta = \frac{1}{\tilde{\chi}} \frac{\partial \mathscr{G}}{\partial \boldsymbol{\sigma}} : \boldsymbol{C} : \operatorname{sym}(\llbracket \dot{\boldsymbol{u}} \rrbracket \otimes \boldsymbol{n}), \quad \tilde{\chi} = \frac{\partial \mathscr{G}}{\partial \boldsymbol{\sigma}} : \boldsymbol{C} : \frac{\partial \mathscr{R}}{\partial \boldsymbol{\sigma}}. \tag{2.25}$$

As before, let $\llbracket \dot{\boldsymbol{u}} \rrbracket = \dot{\zeta} \boldsymbol{m}$. Combining (2.24) and (2.25) gives

$$\dot{\zeta} = \left(\frac{\tilde{\chi}}{\mathscr{H}_\delta} \right) \frac{(\partial \mathscr{G} / \partial \boldsymbol{\sigma}) : \boldsymbol{C} : \operatorname{sym}(\nabla \dot{\overline{\boldsymbol{u}}})}{(\partial \mathscr{G} / \partial \boldsymbol{\sigma}) : \boldsymbol{C} : \operatorname{sym}(\boldsymbol{m} \otimes \boldsymbol{n})}. \tag{2.26}$$

Eq. (2.26) describes the evolution of the jump rate in the bifurcated state.

Clearly, displacement jumps can evolve only when the singular component of the traction vector $\boldsymbol{t}$ remains equal to zero. The evolution condition is (cf. (2.16))

$$\dot{\boldsymbol{t}}_\delta = \dot{\zeta} \boldsymbol{n} \cdot \tilde{\boldsymbol{C}}^{\mathrm{ep}} : \operatorname{sym}(\boldsymbol{m} \otimes \boldsymbol{n}) \equiv \boldsymbol{0}, \tag{2.27}$$

where

$$\tilde{\boldsymbol{C}}^{\mathrm{ep}} = \boldsymbol{C} - \frac{1}{\tilde{\chi}} \boldsymbol{C} : \frac{\partial \mathscr{R}}{\partial \boldsymbol{\sigma}} \otimes \frac{\partial \mathscr{G}}{\partial \boldsymbol{\sigma}} : \boldsymbol{C} \tag{2.28}$$

is the *elastic-perfectly plastic* tangent operator for the damage model. Equivalently, (2.27) can be written as (cf. (2.18))

$$\tilde{\boldsymbol{A}} \cdot \boldsymbol{m} = \boldsymbol{0}, \quad \tilde{\boldsymbol{A}} = \boldsymbol{n} \cdot \tilde{\boldsymbol{C}}^{\mathrm{ep}} \cdot \boldsymbol{n}, \tag{2.29}$$

where $\tilde{\boldsymbol{A}}$ is the elastic-perfectly plastic acoustic tensor in the bifurcated state.

Remark 2. The difference between (2.18) and (2.29) is that the former establishes the condition for the *onset* of displacement jump based on the continuing velocity equation of equilibrium for the intact continuum, whereas the latter sets the condition for the *evolution* of displacement jump based on the constitutive response of a preexisting band. Thus, whereas the unit vectors $\boldsymbol{n}$ and $\boldsymbol{m}$ result from the analysis of the nontrivial solution of (2.18), Eq. (2.29) assumes that these vectors are already well defined, and so the latter equation may simply be used to investigate conditions under which the displacement jump can evolve and continue to be active.

The assumption that plasticity is localized to the discontinuity implies that the continuum unloads just outside the band. Thus, the slip tensor $\mathrm{sym}(\llbracket \dot{\boldsymbol{u}} \rrbracket \otimes \boldsymbol{n})$ must be fully plastic, and so

$$\mathrm{sym}(\llbracket \dot{\boldsymbol{u}} \rrbracket \otimes \boldsymbol{n}) = \lambda_\delta \frac{\partial \mathscr{R}}{\partial \boldsymbol{\sigma}}, \tag{2.30}$$

so that

$$\dot{\boldsymbol{\sigma}} = \boldsymbol{C} : \mathrm{sym}(\nabla \dot{\overline{\boldsymbol{u}}}). \tag{2.31}$$

Eq. (2.30) also has the mathematical significance that $\mathrm{sym}(\llbracket \dot{\boldsymbol{u}} \rrbracket \otimes \boldsymbol{n})$ lies in the null space of $\boldsymbol{C}^{\mathrm{ep}}$, since substituting it in (2.27) results in the satisfaction of the evolution condition $\dot{\boldsymbol{t}}_\delta = \boldsymbol{0}$. In this case, the stress rate $\dot{\boldsymbol{\sigma}}$ just outside the band is given by (2.31) and depends solely on the regular component $\mathrm{sym}(\nabla \dot{\overline{\boldsymbol{u}}})$ of the total strain rate.

Remark 3. Eq. (2.30) is not a contradiction of the point made in Remark 1, which states that $\partial \mathscr{Q} / \partial \boldsymbol{\sigma}$ is not an acceptable form for the tensor $\mathrm{sym}(\llbracket \dot{\boldsymbol{u}} \rrbracket \otimes \boldsymbol{n})$, since $\mathscr{Q}$ and $\mathscr{R}$ could be two entirely different plastic potential functions. If $\mathscr{Q}$ and $\mathscr{R}$ were the same, then (2.30) would not hold and the shear band would not propagate. This statement agrees with the conclusion formulated in [29], where a combined weak–strong discontinuity approach for post-localization analysis was proposed because the band would not propagate with the strong discontinuity model alone when used in conjuction with a J_2-plastic flow. However, this is an unnecessary assumption since there is no reason to suppose that the constitutive response of the intact and damaged continuum must be the same. For example, one can choose a Mohr–Coulomb form for the plastic potential function $\mathscr{R}$ which results in a stress gradient tensor $\partial \mathscr{R} / \partial \boldsymbol{\sigma}$ that possesses exactly two nonzero eignevalues, thereby allowing (2.30) to hold. The point, however, is that a precise form for $\mathscr{R}$ is not even necessary since it will not enter into the formulation anyway. More discussions follow in Section 3.

Assuming (2.30) holds, then we can write

$$\mathrm{sym}(\boldsymbol{m} \otimes \boldsymbol{n}) = \Lambda \frac{\partial \mathscr{R}}{\partial \boldsymbol{\sigma}}, \tag{2.32}$$

where Λ is some proportionality factor. Substituting (2.32) in (2.25) gives

$$\lambda_\delta = \Lambda \dot{\zeta}, \tag{2.33}$$

which means that λ_δ is a linear measure of the slip rate $\dot{\zeta}$. Substituting (2.31) and (2.33) in (2.23) gives

$$\frac{\partial \mathscr{G}}{\partial \boldsymbol{\sigma}} : \dot{\boldsymbol{\sigma}} - \tilde{\mathscr{H}}_\delta \dot{\zeta} = 0, \tag{2.34}$$

where $\tilde{\mathscr{H}}_\delta = \Lambda \mathscr{H}_\delta$ is an alternative softening modulus on the band whose physical significance is elaborated in Remark 4 that follows. Eq. (2.34) is the consistency condition on the band, and states that the stresses just outside the band satisfy the yield condition on the band. The same equation also implies that the stresses on the band are the same as those just outside the band.

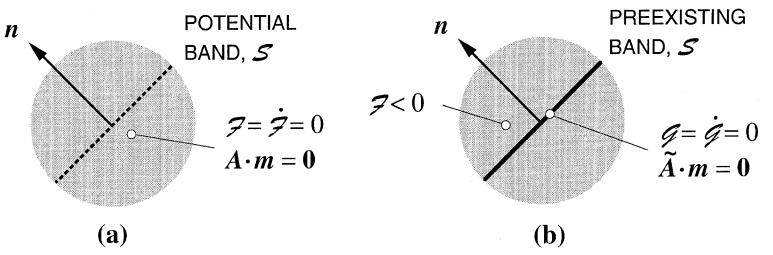

Fig. 1. Dual response of a macroscopic point (shaded region): (a) onset of displacement jump; (b) evolution of displacement jump.

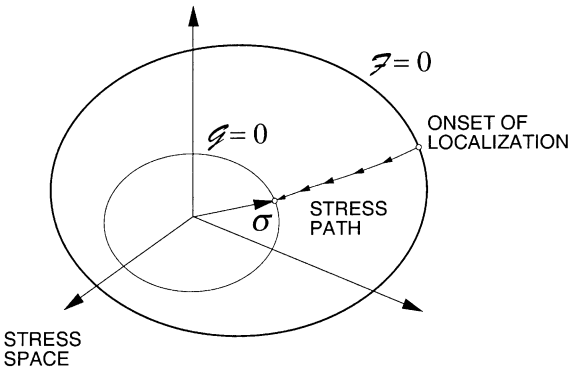

Fig. 2. Evolution of yield and damage functions at post-localization.

Remark 4. The softening modulus $\tilde{\mathscr{H}}_\delta$ relates the rate of softening of the element to the slip rate on the band. As an illustration, consider the case of uniaxial loading in which the only non-zero stress component in the element is the axial stress σ. For a Von Mises material equation (2.34) reduces to $\dot{\sigma}=\tilde{\mathscr{H}}_\delta\dot{\zeta}$, which means that $\tilde{\mathscr{H}}_\delta=\mathrm{d}\sigma/\mathrm{d}\zeta\leqslant 0$ is the slope of the axial stress–total slip curve beyond the bifurcation point. Thus, $\mathscr{H}_\delta$ takes on an analogous meaning to the familiar plastic modulus H' used in deviatoric plasticity theory which relates the effective stress rate $\dot{\bar{\sigma}}$ to the effective plastic strain rate $\dot{\bar{\epsilon}}^{\mathrm{p}}$.

Figs. 1 and 2 provide pictorial representations of the onset and evolution of displacement jumps. Fig. 1(a) shows a macroscopic point on the verge of experiencing a displacement discontinuity across the surface $\mathscr{S}$. This stress point is instantaneously yielding as a continuum, so $\mathscr{F}=\dot{\mathscr{F}}=0$. The localization condition is $\boldsymbol{A}\cdot\boldsymbol{m}=\boldsymbol{0}$, which allows the onset of displacement jump along a surface with unit normal $\boldsymbol{n}$. Fig. 1(b) shows the same macroscopic point during the evolution of the displacement jump. This stress point has $\mathscr{G}=\dot{\mathscr{G}}=0$ on the band, and thus, guarantees yielding along $\mathscr{S}$; however, $\mathscr{F}<0$ just outside the band, implying that the still intact material in the neighborhood of $\mathscr{S}$ has unloaded. The evolution condition is $\tilde{\boldsymbol{A}}\cdot\boldsymbol{m}=\boldsymbol{0}$ on the preexisting band. Fig. 2 shows the dual nature of the response of this macroscopic point during the evolution of the band. Here, the size of the yield function $\mathscr{F}$ is frozen at its value during the onset of localization. However, the damage function $\mathscr{G}=0$ continues to shrink due to the softening response of the stress point on the band.

3. Drucker–Prager model with non-associated plasticity

We now specialize the formulation of the preceding section to a non-associated Drucker–Prager model. This model has been used traditionally to describe the behavior of dilatant frictional materials, such as dense sands and rocks. We provide a closed form expression for the onset of displacement jumps in Drucker–Prager materials under plane strain stress condition, as well as specialize the development of the

post-localization model to include the time-integrated version of the evolution equation for displacement jumps.

3.1. Infinitesimal continuum theory

Consider a free energy function $\Psi(\boldsymbol{\epsilon}^{\mathrm{e}}, \boldsymbol{\xi})$ that is quadratic in both $\boldsymbol{\epsilon}^{\mathrm{e}}$ and $\boldsymbol{\xi}$. Here, the Hessian tensors $\boldsymbol{C}$ and $\boldsymbol{H}$ are both constant, and so Ψ can simply be written as

$$\Psi(\boldsymbol{\epsilon}^{\mathrm{e}}, \boldsymbol{\xi}) = \Psi_0 + \frac{1}{2}\boldsymbol{\epsilon}^{\mathrm{e}} : \boldsymbol{c}^{\mathrm{e}} : \boldsymbol{\epsilon}^{\mathrm{e}} + \frac{1}{2}\boldsymbol{\xi} \cdot \boldsymbol{H} \cdot \boldsymbol{\xi}, \tag{3.1}$$

where Ψ_0 is a scalar constant, and $\boldsymbol{c}^{\mathrm{e}}$ is the usual rank-four elastic stress–strain tensor, which, for isotropic elastic material, takes the form

$$\boldsymbol{c}^{\mathrm{e}} = K\mathbf{1} \otimes \mathbf{1} + 2\mu\left(\boldsymbol{I} - \frac{1}{3}\mathbf{1} \otimes \mathbf{1}\right), \tag{3.2}$$

where K and μ are the (constant) elastic bulk and shear moduli, respectively, $\mathbf{1}$ is the Kronecker delta tensor, and I is the rank-four identity tensor. Now, take $\boldsymbol{\xi} \in \mathbb{R}^2$ as a vector of plastic internal variables containing volumetric and deviatoric plastic strains, defined as

$$\boldsymbol{\xi} := \begin{Bmatrix} v^{\mathrm{p}} \\ e^{\mathrm{p}} \end{Bmatrix}, \quad \boldsymbol{H} = \begin{bmatrix} K' & 0 \\ 0 & H' \end{bmatrix}, \quad \boldsymbol{\theta} = \begin{Bmatrix} \theta_1 \\ \theta_2 \end{Bmatrix} = -\frac{\partial \Psi}{\partial \boldsymbol{\xi}} = -\boldsymbol{H}\boldsymbol{\xi}, \tag{3.3}$$

where K' and H' are plastic bulk and shear moduli, respectively, and

$$\dot{v}^{\mathrm{p}} = \mathrm{tr}(\dot{\boldsymbol{\epsilon}}^{\mathrm{p}}), \quad \dot{e}^{\mathrm{p}} = \sqrt{\frac{2}{3}}\|\dot{\boldsymbol{e}}^{\mathrm{p}}\|, \quad \dot{\boldsymbol{e}}^{\mathrm{p}} = \dot{\boldsymbol{\epsilon}}^{\mathrm{p}} - \dot{v}^{\mathrm{p}}\frac{\mathbf{1}}{3}, \quad v^{\mathrm{p}} = \int_t \dot{v}^{\mathrm{p}}\,\mathrm{d}t, \quad e^{\mathrm{p}} = \int_t \dot{e}^{\mathrm{p}}\,\mathrm{d}t. \tag{3.4}$$

More complex hardening/softening laws, such as a bilogarithmic compressibility relationship between the plastic variables θ_1 and v^{p} for soils, can be postulated [30–32], but these details are not central to the theory and may be omitted in the present discussion.

The Drucker–Prager yield function takes the form

$$\mathscr{F}(\boldsymbol{\sigma}, \boldsymbol{\theta}) = \sqrt{\frac{3}{2}}\|\boldsymbol{s}\| - \sqrt{3}(\alpha - \beta p) = 0, \tag{3.5}$$

where

$$p = \frac{1}{3}\mathrm{tr}(\boldsymbol{\sigma}), \quad \boldsymbol{s} = \boldsymbol{\sigma} - p\mathbf{1}, \tag{3.6}$$

and (α, β) are material parameters which are related to the cohesion $\overline{c}$ and angle of internal friction $\overline{\phi}$ commonly used to describe a Mohr–Coulomb material [33]. The parameters α and β depend on the cohesion $\overline{c}$ and friction angle $\overline{\phi}$ through the relationship of the form [32]

$$\alpha = \frac{6\overline{c}\cos\overline{\phi}}{\sqrt{3}(3 \pm \sin\overline{\phi})}, \quad \beta = \frac{6\sin\overline{\phi}}{\sqrt{3}(3 \pm \sin\overline{\phi})}, \tag{3.7}$$

where the $\pm$-sign depends on whether the Drucker–Prager cone is completely inscribed in or completely circumscribes the Mohr–Coulomb hexagon. A constant β then implies a constant angle of internal friction $\overline{\phi}$. However, in this paper we will allow α to vary with plastic deformation, so that, in effect, the cone generated by (3.5) in principal stress space retains its shape and proportion but not its size.

Now, consider a plastic potential of the form

$$\mathscr{Q}(\boldsymbol{\sigma}, \boldsymbol{\theta}) = \sqrt{\frac{3}{2}}\|\boldsymbol{s}\| - \sqrt{3}(\alpha - bp), \tag{3.8}$$

where $b \geqslant 0$ is another material constant whose physical significance is elaborated in the next section. Defining

$$\alpha := \alpha_0 + b\theta_1 + \frac{1}{\sqrt{3}}\theta_2, \tag{3.9}$$

where α_0 is constant, and (θ_1, θ_2) are the elements of the vector $\boldsymbol{\theta}$ as defined in $(3.3)_3$, we see that

$$\dot{\boldsymbol{\xi}} = \lambda \frac{\partial \mathscr{Q}}{\partial \boldsymbol{\theta}} = \lambda \frac{\partial \mathscr{F}}{\partial \boldsymbol{\theta}} = -\lambda \begin{Bmatrix} \sqrt{3}b \\ 1 \end{Bmatrix}, \tag{3.10}$$

and so the model is associative with respect to hardening. On the other hand, $b = \beta$ implies associative plasticity, but a non-associated model can always be constructed by choosing $b \neq \beta$. The expression for the hardening parameter $\mathscr{H}$ thus simplifies to

$$\mathscr{H} = 3b^2K' + H'. \tag{3.11}$$

We next recall the following expression for the hardening modulus that allows for the development of singular solutions on the band

$$\mathscr{H}^{-1} = \mathscr{H}_\delta^{-1}\delta_{\mathscr{S}}, \quad \mathscr{H}_\delta = 3b^2K_\delta + H_\delta, \tag{3.12}$$

where K_δ and H_δ are the plastic moduli on the band (equivalent to the continuum moduli K' and H' in the intact state). In general, the elaborate expressions (3.11) and (3.12) are not necessary since it only suffices to specify the parameters $\mathscr{H}$ and $\mathscr{H}_\delta$ in the analysis.

3.2. Localization condition in plane strain

Following the procedure of the previous section, let us now evaluate relevant expressions leading to the condition for the onset of displacement jumps. The gradients of $\mathscr{F}$ and $\mathscr{Q}$ with respect to stresses may be evaluated readily as

$$\frac{\partial \mathscr{F}}{\partial \boldsymbol{\sigma}} = \sqrt{\frac{3}{2}}\,\hat{\boldsymbol{n}} + \frac{1}{\sqrt{3}}\beta\mathbf{1}, \quad \frac{\partial \mathscr{Q}}{\partial \boldsymbol{\sigma}} = \sqrt{\frac{3}{2}}\,\hat{\boldsymbol{n}} + \frac{1}{\sqrt{3}}b\mathbf{1}, \tag{3.13}$$

where $\hat{\boldsymbol{n}} = \boldsymbol{s}/\|\boldsymbol{s}\|$. The elastic-perfectly plastic tangent operator is

$$\boldsymbol{C}^{\mathrm{ep}} = \boldsymbol{C}^{\mathrm{e}} - \boldsymbol{C}^{\mathrm{p}}, \tag{3.14}$$

where

$$\boldsymbol{C}^{\mathrm{e}} = K\mathbf{1}\otimes\mathbf{1} + 2\mu\left(\boldsymbol{I} - \frac{1}{3}\mathbf{1}\otimes\mathbf{1}\right) \tag{3.15}$$

is the elastic component of $\boldsymbol{C}^{\mathrm{ep}}$, and

$$\boldsymbol{C}^{\mathrm{p}} = \frac{1}{\chi}\left[\beta bK^2\mathbf{1}\otimes\mathbf{1} + \sqrt{2}\mu K(\beta\hat{\boldsymbol{n}}\otimes\mathbf{1} + b\mathbf{1}\otimes\hat{\boldsymbol{n}}) + 2\mu^2\hat{\boldsymbol{n}}\otimes\hat{\boldsymbol{n}}\right] \tag{3.16}$$

is the plastic part, with $\chi = \beta bK + \mu$.

The corresponding elastic-perfectly plastic acoustic tensor is

$$\boldsymbol{A} = \boldsymbol{A}^{\mathrm{e}} - \boldsymbol{A}^{\mathrm{p}}, \tag{3.17}$$

where

$$\boldsymbol{A}^{\mathrm{e}} = \boldsymbol{n}\cdot\boldsymbol{C}^{\mathrm{e}}\cdot\boldsymbol{n} = \left(K + \frac{\mu}{3}\right)\boldsymbol{n}\otimes\boldsymbol{n} + \mu\mathbf{1} \tag{3.18}$$

is the elastic part of $\boldsymbol{A}$, and

$$\boldsymbol{A}^{\mathrm{p}} = \boldsymbol{n}\cdot\boldsymbol{C}^{\mathrm{p}}\cdot\boldsymbol{n} = \frac{1}{\chi}\left[\beta b K^2 \boldsymbol{n}\otimes\boldsymbol{n} + \sqrt{2}\mu K(\beta\boldsymbol{N}\otimes\boldsymbol{n} + b\boldsymbol{n}\otimes\boldsymbol{N}) + 2\mu^2\boldsymbol{N}\otimes\boldsymbol{N}\right] \tag{3.19}$$

is the plastic part, with $\boldsymbol{N} = \hat{\boldsymbol{n}}\cdot\boldsymbol{n} = \boldsymbol{n}\cdot\hat{\boldsymbol{n}}$. Note that neither $\boldsymbol{C}^{\mathrm{ep}}$ nor $\boldsymbol{A}$ has a major symmetry unless $\beta = b$. Since a necessary condition for the onset of displacement jump is $\boldsymbol{A}\cdot\boldsymbol{m} = \boldsymbol{0}$, it is necessary that $\det(\boldsymbol{A}) = 0$ for non-trivial solutions to exist.

For plane strain localization on the plane (x_1, x_2), the tensor $\boldsymbol{A}$ has the structure

$$\boldsymbol{A} = \begin{bmatrix} \tilde{\boldsymbol{A}} & \boldsymbol{0} \\ \boldsymbol{0} & \mu \end{bmatrix}, \quad \tilde{\boldsymbol{A}} = \begin{bmatrix} A_{11} & A_{12} \\ A_{21} & A_{22} \end{bmatrix}. \tag{3.20}$$

This results from imposing the condition that the vector $\boldsymbol{n}$ should have the null element $n_3 = 0$, which in turn implies that $\boldsymbol{N}$ has the null element $N_3 = 0$. Thus, the slip direction $\boldsymbol{m}$ must also have the null element $m_3 = 0$ or the localization condition will not be satisfied. The slip vector $\boldsymbol{m}$ with $m_3 = 0$ satisfies the kinematics of plane strain deformation, as well as results in the slip tensor having the property that $\mathrm{sym}(\boldsymbol{m}\otimes\boldsymbol{n})_{ij} = \mathrm{sym}(m_i n_j) = 0$ whenever $i = 3$ or $j = 3$.

Since $m_3 = 0$, then non-trivial solutions can exist if and only if

$$\tilde{\boldsymbol{A}}\cdot\tilde{\boldsymbol{m}} = \boldsymbol{0} \Rightarrow \det(\tilde{\boldsymbol{A}}) = 0, \tag{3.21}$$

where $\tilde{\boldsymbol{m}} = \{m_1, m_2\}$. A closed form solution to the zero-determinant condition for the plane-strain problem is available, as shown in [17]. The idea is to consider the right eigenvalue problem

$$\tilde{\boldsymbol{A}}\cdot\tilde{\boldsymbol{m}} = \lambda\tilde{\boldsymbol{A}}^{\mathrm{e}}\cdot\tilde{\boldsymbol{m}} \tag{3.22}$$

and then premultiplying (3.22) by the inverse, $(\tilde{\boldsymbol{A}}^{\mathrm{e}})^{-1}$, to obtain the standard eigenvalue problem

$$\boldsymbol{B}\cdot\tilde{\boldsymbol{m}} = \lambda\tilde{\boldsymbol{m}}, \tag{3.23}$$

where $\boldsymbol{B} = (\tilde{\boldsymbol{A}}^{\mathrm{e}})^{-1}\tilde{\boldsymbol{A}}$. The inversion is always possible since $\tilde{\boldsymbol{A}}^{\mathrm{e}}$ is positive definite, see (3.18). One eigenvalue of $\boldsymbol{B}$ is $\lambda^{(1)} = 1$, which corresponds to the elastic eigenmode [17], while the second eigenvalue is $\lambda^{(2)} = 1 - (\tilde{\boldsymbol{A}}^{\mathrm{e}})^{-1} : \tilde{\boldsymbol{A}}^{\mathrm{p}}$, which corresponds to the localization mode. Setting $\lambda^{(2)} = 0$ then guarantees a singular $\boldsymbol{B}$, which in turn implies a singular $\tilde{\boldsymbol{A}}$. This condition is equivalent to the scalar expression (cf. (82) of [17])

$$h = 2(\beta - b)^2 - (1 - \nu)\left(\frac{3\sqrt{2}s_3}{\|\boldsymbol{s}\|} + \beta + b\right)^2 = 0, \tag{3.24}$$

where $s_3 = \sigma_3 - p$ is the (3, 3)-normal component of the deviatoric stress tensor $\boldsymbol{s}$, and ν is the elastic Poisson's ratio.

Eq. (3.24) ensures the initial vanishing of the determinant of $\tilde{\boldsymbol{A}}$. Over a finite time-step the localization condition can be detected by checking to see if the sign of h reverses during a given loading increment, i.e., if $h_n h_{n+1} < 0$ over the time interval $t_n < t < t_{n+1}$. If it does, then $\det(\tilde{\boldsymbol{A}})$ crosses the value of zero within this critical time interval for some orientation of the unit normal vector $\boldsymbol{n}$. Equivalently, one can monitor the absolute value of h as defined in (3.24) to see if it falls below some maximum allowable value, as elaborated further in Section 5, to activate the localization mode. The angle θ that $\boldsymbol{n}$ makes with respect to the major principal stress in compression, σ_1, is equal to the angle that the slip surface makes with respect to the minor principal stress in compression, σ_2, and is given by the expression (cf. (80) of [17])

$$\tan^2\theta = -\frac{c_2}{c_1}, \tag{3.25}$$

where

$$c_1 = 3(s_1 + \nu s_3) + (1 + \nu)(\beta + b)\|\boldsymbol{s}\|/\sqrt{2} < 0, \tag{3.26a}$$

$$c_2 = 3(s_2 + \nu s_3) + (1 + \nu)(\beta + b)\|\boldsymbol{s}\|/\sqrt{2} > 0. \tag{3.26b}$$

The inequalities in (3.26a) and (3.26b) must be satisfied in order for (3.25) to provide real roots. This is possible provided that β and b fall within some permissible values, and that the stresses are chosen such that $s_1 = \sigma_1 - p,\ s_2 = \sigma_2 - p$, and the ordering is $s_1 < s_3 < s_2$. Fig. 3 shows the meaning of the angle θ relative to the directions of the major and minor principal stresses in compression.

The eigenvector $\tilde{\boldsymbol{m}}$ satisfies the characteristic equation and defines the direction of the slip rate at the onset of localization. Noting that $\tilde{\boldsymbol{m}} = \{m_1, m_2\}$ and $m_2 = \pm(1 - m_1^2)^{-1/2}$, we can readily substitute this eigenvector into the characteristic equation (3.21) to obtain

$$m_1 = \pm \frac{A_{12}}{\sqrt{A_{11}^2 + A_{12}^2}} \quad \text{or} \quad m_1 = \pm \frac{A_{22}}{\sqrt{A_{21}^2 + A_{22}^2}} \tag{3.27a}$$

and

$$m_2 = \mp \frac{A_{11}}{\sqrt{A_{11}^2 + A_{12}^2}} \quad \text{or} \quad m_2 = \mp \frac{A_{21}}{\sqrt{A_{21}^2 + A_{22}^2}}. \tag{3.27b}$$

Provided that $\tilde{\boldsymbol{A}}$ is singular, the components of $\tilde{\boldsymbol{m}}$ can be calculated from either expression in Eqs. (3.27a) and (3.27b), which should yield the same result.

Remark 5. The sign of $\boldsymbol{m}$ can be chosen so that $\sin\psi = \boldsymbol{n} \cdot \boldsymbol{m} > 0$, where ψ is the dilatancy angle representing the angle that $\boldsymbol{m}$ makes with respect to the slip surface $\mathscr{S}$ (see Fig. 4). This guarantees a dilatant behavior and prevents overlapping of the sliding elements. Thus, a unique eigenvector $\boldsymbol{m}$ can be associated

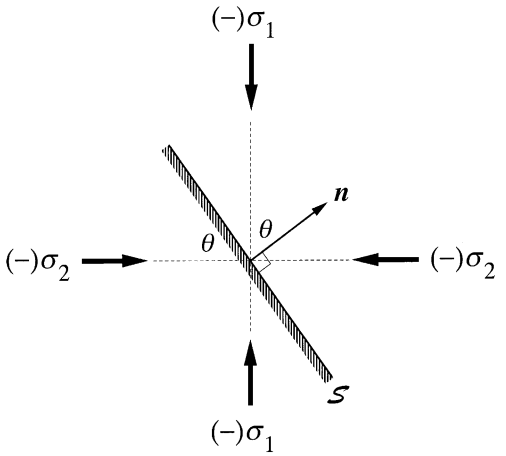

Fig. 3. Orientations of slip line $\mathscr{S}$ and unit normal $\boldsymbol{n}$.

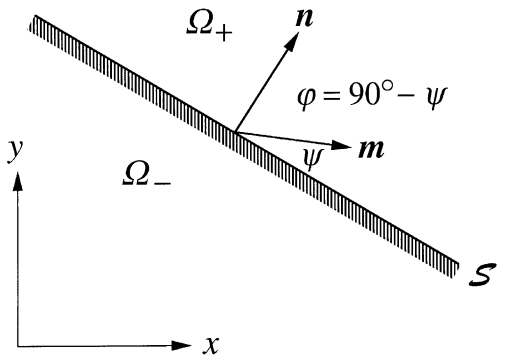

Fig. 4. Displacement jump direction $\boldsymbol{m}$ and dilatancy angle ψ.

with a unit normal vector $\boldsymbol{n}$ to result in a dilatant behavior at the onset of localization. However, there are always two possible unit vectors $\boldsymbol{n}$ that can be extracted from (3.25) depending on the sign chosen for the angle θ. In this case, the sign of θ is chosen so that the slip surface orientation conforms with the instantaneous displacement gradient of the localizing element at the onset of localization, i.e., $\boldsymbol{n}$ is chosen so that $\nabla \boldsymbol{u} : (\boldsymbol{m} \otimes \boldsymbol{n})$ is maximized. Clearly, no unique solution can be found if $\nabla \boldsymbol{u}$ is symmetric, but for non-symmetric displacement gradient its rotational component can be used to determine uniquely the desired direction $\boldsymbol{n}$.

3.3. Post-localization model

To be able to advance the solution beyond the point of localization, it is necessary to formulate a damage model. In doing so it is again important to remember that once an element has localized both the yield and plastic potential functions in the intact state deactivate, and new yield and plastic potential functions take effect reflecting the bifurcated constitutive response of the element in the damaged state.

Let us consider a damage model given by the function

$$\mathscr{G} = \operatorname{sym}(\boldsymbol{n} \otimes \boldsymbol{l}) : \boldsymbol{\sigma} - [\mathscr{A} - (\boldsymbol{n} \otimes \boldsymbol{n}) : \boldsymbol{\sigma} \tan \phi_{\mathscr{S}}] = 0, \tag{3.28}$$

where $\boldsymbol{l}$ is the unit tangent vector to the band, $\phi_{\mathscr{S}}$ the mobilized friction angle on the band (not to be confused with the angle $\overline{\phi}$ used in (3.7) for the intact continuum), and $\mathscr{A}$ is the size of $\mathscr{G}$ which takes on the initial value

$$\mathscr{A}_0 = \operatorname{sym}(\boldsymbol{n} \otimes \boldsymbol{l}) : \boldsymbol{\sigma}^* + (\boldsymbol{n} \otimes \boldsymbol{n}) : \boldsymbol{\sigma}^* \tan \phi_{\mathscr{S}}, \tag{3.29}$$

where $\boldsymbol{\sigma}^*$ is the value of $\boldsymbol{\sigma}$ at the onset of localization. We assume that $\phi_{\mathscr{S}}$ is constant but accommodate a softening response by allowing $\mathscr{A}$ to vary. Eq. (3.28) has the physical significance that slip on $\mathscr{S}$ occurs when the resolved tangential shear stress reaches a certain maximum value, and that this maximum value is proportional to the normal compressive stress acting on $\mathscr{S}$. For future use, the stress gradient of the function $\mathscr{G}$ is given by

$$\frac{\partial \mathscr{G}}{\partial \boldsymbol{\sigma}} = \operatorname{sym}(\boldsymbol{n} \otimes \boldsymbol{\mu}), \quad \boldsymbol{\mu} = \boldsymbol{l} + \boldsymbol{n} \tan \phi_{\mathscr{S}}. \tag{3.30}$$

As for the damage function $\mathscr{R}$, Remark 3 indicates that a precise form for this function is not necessary since

$$\frac{\partial \mathscr{R}}{\partial \boldsymbol{\sigma}} \propto \operatorname{sym}(\boldsymbol{m} \otimes \boldsymbol{n}), \tag{3.31}$$

and $\operatorname{sym}(\boldsymbol{m} \otimes \boldsymbol{n})$ has already been evaluated at the onset of localization. However, (3.31) assumes that the dilatancy angle at the onset of localization persists at post-localization. If this is not the case, then $\mathscr{R}$ can be suitably defined to reflect the evolution of the dilatancy angle at post-localization, for example, through some form of variation of the slip direction $\boldsymbol{m}$ at post-localization.

4. Finite element implementation

For simplicity, we will restrict the development below to quasi-static problems under the assumption of infinitesimal deformation. A first step in the finite element implementation is the development of the weak form of the governing equilibrium equations. The reader is referred to [1,13,14] for details of the mathematical formulation. To avoid repetition, we will simply summarize important details of the formulation and point out essential modifications to the governing weak equation that make the model suitable for the two-invariant, non-associated Drucker–Prager theory described in the preceding section.

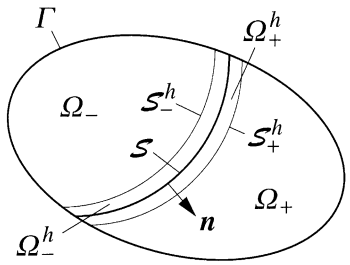

Fig. 5. Definition of surface of discontinuity.

4.1. Weak form

Consider a reparameterized displacement field $\boldsymbol{u}$ of the form

$$\boldsymbol{u} = \overline{\boldsymbol{u}} + [\![\boldsymbol{u}]\!] M_{\mathscr{S}}. \tag{4.1}$$

The jump of $M_{\mathscr{S}}$ across $\mathscr{S}$ is $[\![M_{\mathscr{S}}]\!] = 1$, with $M_{\mathscr{S}} = 0$ on the surface $\mathscr{S}_{\pm}^h$ of its (compact) support $\Omega^h = \Omega_+^h \cup \Omega_-^h$, see Fig. 5. In terms of the Heaviside function $H_{\mathscr{S}}$, the jump function $M_{\mathscr{S}}$ may be represented as

$$M_{\mathscr{S}} = H_{\mathscr{S}} - f^h, \tag{4.2}$$

where f^h is any arbitrary smooth function that satisfies the requirements $f^h = 0$ in $\Omega_- \setminus \Omega_-^h$, and $f^h = 1$ in $\Omega_+ \setminus \Omega_+^h$, see Fig. 5.

The weighting function $\boldsymbol{\eta}$ may be expressed in the same reparameterized form

$$\boldsymbol{\eta} = \overline{\boldsymbol{\eta}} + [\![\boldsymbol{\eta}]\!] M_{\mathscr{S}}, \tag{4.3}$$

where $[\![\boldsymbol{\eta}]\!]$ is the variation jump on $\mathscr{S}$. Here, $\overline{\boldsymbol{\eta}}$ satisfies the usual boundary condition $\overline{\boldsymbol{\eta}} = \boldsymbol{0}$ on the part of the boundary Γ where $\boldsymbol{u}$ is prescribed (essential boundary condition). Using the weighting function $\boldsymbol{\eta}$, the variational equation in rate form can be written as

$$\int_{\Omega} \nabla \boldsymbol{\eta} : \dot{\boldsymbol{\sigma}} \, \mathrm{d}\Omega - \int_{\Omega} \boldsymbol{\eta} \cdot \dot{\boldsymbol{f}} \, \mathrm{d}\Omega - \int_{\Gamma} \boldsymbol{\eta} \cdot \dot{\boldsymbol{t}} \, \mathrm{d}\Gamma = \boldsymbol{0}, \tag{4.4}$$

where $\dot{\boldsymbol{f}}$ and $\dot{\boldsymbol{t}}$ are the prescribed body force and traction rate vectors, respectively.

In [18], it was shown that (4.4) is equivalent to the standard local equilibrium equations

$$\mathrm{div}(\dot{\boldsymbol{\sigma}}) + \dot{\boldsymbol{f}} = \boldsymbol{0} \quad \text{in } \Omega \setminus \mathscr{S} \qquad \text{and} \qquad \dot{\boldsymbol{\sigma}} \cdot \boldsymbol{v} = \dot{\boldsymbol{t}} \quad \text{on } \Gamma_{\mathrm{t}} \tag{4.5}$$

in which $\boldsymbol{v}$ is the outward unit normal to the surface Γ_{t}, where the traction rate vector $\dot{\boldsymbol{t}}$ is prescribed. Since the domain of validity of $(4.5)_1$ excludes the surface $\mathscr{S}$, the equations are supplemented by the conditions

$$(\dot{\boldsymbol{\sigma}}_+ - \dot{\boldsymbol{\sigma}}_-) \cdot \boldsymbol{n} = \boldsymbol{0} \quad \text{and} \quad \dot{\boldsymbol{\sigma}}_{\mathscr{S}} \cdot \boldsymbol{n} = \dot{\boldsymbol{\sigma}}_+ \cdot \boldsymbol{n}, \tag{4.6}$$

where $\dot{\boldsymbol{\sigma}}_{\mathscr{S}} \cdot \boldsymbol{n}$ denotes the traction rate vector acting on the surface $\mathscr{S}$. Relations (4.6) imply that the jump of the traction rate vector across $\mathscr{S}$ is zero, and that the traction rate vector acting on the surface of discontinuity $\mathscr{S}$ is equal to the traction rate vector acting on the continuum located adjacent to $\mathscr{S}$.

4.2. Finite element approximations

The finite element approximations are based on the weak equations resulting from the assumed enhanced strain method [18,19]

$$\int_{\Omega} \mathrm{sym}(\nabla \overline{\boldsymbol{\eta}}^h) : \dot{\boldsymbol{\sigma}}\, \mathrm{d}\Omega = \int_{\Omega} \overline{\boldsymbol{\eta}}^h \cdot \dot{\boldsymbol{f}}\, \mathrm{d}\Omega + \int_{\Gamma} \overline{\boldsymbol{\eta}}^h \cdot \dot{\boldsymbol{t}}\, \mathrm{d}\Gamma, \tag{4.7a}$$

$$\int_{\Omega^{\mathrm{e}}_{\mathrm{loc}}} \tilde{\boldsymbol{\gamma}}^h : \dot{\boldsymbol{\sigma}}\, \mathrm{d}\Omega = 0 \quad \forall e \in \{\text{set of localized elements}\}, \tag{4.7b}$$

where $\mathrm{sym}(\nabla \overline{\boldsymbol{\eta}}^h)$ represents the compatible component of the total strain variation, and $\tilde{\boldsymbol{\gamma}}^h$ represents the assumed enhanced component. Eq. (4.7a) is the usual weak statement of balance of momentum, while (4.7b) defines the nature of the enhancement for the localized elements. In order for $\tilde{\boldsymbol{\gamma}}^h$ to enhance the compatible strain field, $\mathrm{sym}(\nabla \overline{\boldsymbol{\eta}}^h)$, their spaces must have a null intersection [19].

We now consider two cases. The first has $[\![\boldsymbol{u}]\!] = [\![\boldsymbol{\eta}]\!] = \boldsymbol{0}$ in Ω^{e}. Thus $\boldsymbol{\eta}^h = \overline{\boldsymbol{\eta}}^h$, and so (4.7a) reverts back to the standard weak statement of balance of momentum in Ω^{e} with no displacement jumps, and the element is not enhanced. The second and more relevant case has $[\![\boldsymbol{u}]\!] = \zeta^{\mathrm{e}} \boldsymbol{m} \neq \boldsymbol{0}$ with $\zeta^{\mathrm{e}} \neq 0$ representing the total strength of the jump in Ω^{e}. In this case, the small strain tensor becomes

$$\boldsymbol{\epsilon}^h_{\mathrm{e}} = \mathrm{cnf}(\boldsymbol{\epsilon}^h_{\mathrm{e}}) + \mathrm{enh}(\boldsymbol{\epsilon}^h_{\mathrm{e}}) = \mathrm{reg}(\boldsymbol{\epsilon}^h_{\mathrm{e}}) + \mathrm{sng}(\boldsymbol{\epsilon}^h_{\mathrm{e}}), \tag{4.8}$$

where "cnf" denotes conforming, "enh" enhanced, "reg" regular, and "sng" denotes singular parts, which are given explicitly by

$$\mathrm{cnf}(\boldsymbol{\epsilon}^h_{\mathrm{e}}) = \mathrm{sym}(\nabla \overline{\boldsymbol{u}}^h), \tag{4.9a}$$

$$\mathrm{enh}(\boldsymbol{\epsilon}^h_{\mathrm{e}}) = \zeta^{\mathrm{e}} \mathrm{sym}(\boldsymbol{n} \otimes \boldsymbol{m}) \delta_{\mathscr{S}} - \zeta^{\mathrm{e}} \mathrm{sym}(\nabla f^h_{\mathrm{e}} \otimes \boldsymbol{m}), \tag{4.9b}$$

$$\mathrm{reg}(\boldsymbol{\epsilon}^h_{\mathrm{e}}) = \mathrm{sym}(\nabla \overline{\boldsymbol{u}}^h) - \zeta^{\mathrm{e}} \mathrm{sym}(\nabla f^h_{\mathrm{e}} \otimes \boldsymbol{m}), \tag{4.9c}$$

$$\mathrm{sng}(\boldsymbol{\epsilon}^h_{\mathrm{e}}) = \zeta^{\mathrm{e}} \mathrm{sym}(\boldsymbol{n} \otimes \boldsymbol{m}) \delta_{\mathscr{S}}. \tag{4.9d}$$

Thus

$$\dot{\boldsymbol{\sigma}} = \boldsymbol{c}^{\mathrm{e}} : \mathrm{reg}(\dot{\boldsymbol{\epsilon}}^h_{\mathrm{e}}). \tag{4.10}$$

The particular case, where $[\![\boldsymbol{u}]\!] \neq \boldsymbol{0}$ requires the construction of the weighting function $\tilde{\boldsymbol{\gamma}}^h$ for use in the weak Eq. (4.7b).

Let us set

$$\tilde{\boldsymbol{\gamma}}^h = \boldsymbol{\xi} \left[\frac{\ell^{\mathrm{e}}_{\mathscr{S}}}{A_{\mathrm{e}}} \boldsymbol{\psi} - \boldsymbol{\psi} \delta_{\mathscr{S}} \right], \quad \boldsymbol{\psi} = \frac{\partial \mathscr{G}}{\partial \boldsymbol{\sigma}}, \quad \boldsymbol{\xi} \in R^1, \tag{4.11}$$

where A_{e} is the area of the element $\Omega^{\mathrm{e}}_{\mathrm{loc}}$, and $\ell^{\mathrm{e}}_{\mathscr{S}}$ is the length of the discontinuity line (see Fig. 6). This weighting function satisfies the stability and consistency (patch test) conditions set forth in [19] for

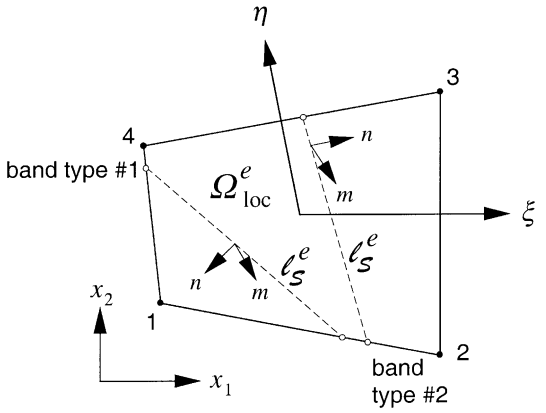

Fig. 6. Slip in a bilinear quadrilateral element.

convergence of enhanced strain methods. For the damage model presented in Section 3.3, a specific form for $\boldsymbol{\psi}$ is given by (3.30).

Substituting (4.11) in (4.7b), and taking note that $\boldsymbol{\xi}$ is an arbitrary non-zero scalar function, we obtain

$$\frac{\ell^{\mathrm{e}}_{\mathscr{S}}}{A^{\mathrm{e}}}\int_{\Omega^{\mathrm{e}}_{\mathrm{loc}}}\boldsymbol{\psi}:\dot{\boldsymbol{\sigma}}\,\mathrm{d}\Omega=\int_{\mathscr{S}^{\mathrm{e}}}\boldsymbol{\psi}:\dot{\boldsymbol{\sigma}}\,\mathrm{d}\mathscr{S}=\ell^{\mathrm{e}}_{\mathscr{S}}\boldsymbol{\psi}:\dot{\boldsymbol{\sigma}}, \tag{4.12}$$

assuming that $\boldsymbol{\psi}:\dot{\boldsymbol{\sigma}}$ is constant along $\mathscr{S}^{\mathrm{e}}$. Thus, from (2.34)

$$\frac{1}{A^{\mathrm{e}}}\int_{\Omega^{\mathrm{e}}_{\mathrm{loc}}}\boldsymbol{\psi}:\dot{\boldsymbol{\sigma}}\,\mathrm{d}\Omega=\tilde{\mathscr{H}}_{\delta}\dot{\zeta}. \tag{4.13}$$

Eq. (4.13) implies that the enhancement to the finite element equations is provided by the consistency condition on the band.

4.3. Matrix equations

Consider the following standard element matrix substitutions:

$$\overline{\boldsymbol{\eta}}^{h}\rightarrow\boldsymbol{N}\boldsymbol{\phi}^{\mathrm{e}},\quad\nabla\overline{\boldsymbol{\eta}}^{h}\rightarrow\boldsymbol{B}\boldsymbol{\phi}^{\mathrm{e}},\quad\boldsymbol{\psi}\rightarrow\boldsymbol{F},\quad\mathrm{sym}(\nabla f^{h}_{\mathrm{e}}\otimes\boldsymbol{m})\rightarrow\boldsymbol{G},\quad\boldsymbol{c}^{\mathrm{e}}\rightarrow\boldsymbol{D}^{\mathrm{e}}, \tag{4.14}$$

where $\boldsymbol{\phi}^{\mathrm{e}}\in\mathbb{R}^{n_{\mathrm{ed}}}$ is an arbitrary vector of nodal displacements, and n_{ed} is the number of element displacement degrees of freedom. With a slight abuse in notation, we will denote in the following the stress rate tensor and its vectorized form by the same symbol $\dot{\boldsymbol{\sigma}}$.

We again consider two cases. The first has $[\![\boldsymbol{u}]\!]=[\![\boldsymbol{\eta}]\!]=\boldsymbol{0}$, and so we revert back to the standard weak statement of balance of momentum (4.7a), which, in time-integrated matrix form, reads

$$\boldsymbol{r}^{\mathrm{e}}=\int_{\Omega^{\mathrm{e}}}\boldsymbol{B}^{t}\boldsymbol{\sigma}\,\mathrm{d}\Omega-\int_{\Omega^{\mathrm{e}}}\boldsymbol{N}^{t}\boldsymbol{f}\,\mathrm{d}\Omega-\int_{\Gamma^{\mathrm{e}}}\boldsymbol{N}^{t}\boldsymbol{t}\,\mathrm{d}\Gamma=\boldsymbol{0}. \tag{4.15}$$

In this case the displacement jumps are zero, and the element is not enhanced. The second and more relevant case has $[\![\boldsymbol{u}]\!]\neq\boldsymbol{0}$. In this case, (4.15) is imposed in $\Omega^{\mathrm{e}}_{\mathrm{loc}}$, and is augmented by the scalar Eq. (4.13), which, in incremental form, reads

$$b^{\mathrm{e}}=\frac{1}{A^{\mathrm{e}}}\int_{\Omega^{\mathrm{e}}_{\mathrm{loc}}}\boldsymbol{F}^{t}\Delta\boldsymbol{\sigma}\,\mathrm{d}\Omega-\tilde{\mathscr{H}}_{\delta}\Delta\zeta^{\mathrm{e}}=0. \tag{4.16}$$

Here, $\Delta\zeta^{\mathrm{e}}$ is the incremental strength of the jump, which may be assumed constant in $\Omega^{\mathrm{e}}_{\mathrm{loc}}$ but discontinuous across the elements. For simplicity in implementation, we will evaluate $\boldsymbol{F}^{t}$ at the beginning of the time increment and assume that it is constant over the time interval in question (explicit treatment).

Consider now the case where $[\![\boldsymbol{u}]\!]\neq\boldsymbol{0}$. Here, the linearizations of (4.15) and (4.16) for the case of dead, monotonic loading [34] are

$$\delta\boldsymbol{r}^{\mathrm{e}}=\boldsymbol{K}^{\mathrm{e}}_{dd}\delta\boldsymbol{d}^{\mathrm{e}}+\boldsymbol{K}^{\mathrm{e}}_{d\zeta}\delta\zeta^{\mathrm{e}}, \tag{4.17a}$$

$$\delta b^{\mathrm{e}}=\boldsymbol{K}^{\mathrm{e}}_{\zeta d}\delta\boldsymbol{d}^{\mathrm{e}}+K^{\mathrm{e}}_{\zeta\zeta}\delta\zeta^{\mathrm{e}}, \tag{4.17b}$$

where

$$\begin{aligned}&\boldsymbol{K}^{\mathrm{e}}_{dd}=\int_{\Omega^{\mathrm{e}}_{\mathrm{loc}}}\boldsymbol{B}^{t}\boldsymbol{D}^{\mathrm{e}}\boldsymbol{B}\,\mathrm{d}\Omega,\quad\boldsymbol{K}_{d\zeta}=-\int_{\Omega^{\mathrm{e}}_{\mathrm{loc}}}\boldsymbol{B}^{t}\boldsymbol{D}^{\mathrm{e}}\boldsymbol{G}\,\mathrm{d}\Omega,\\&\boldsymbol{K}_{\zeta d}=\frac{1}{A^{\mathrm{e}}}\int_{\Omega^{\mathrm{e}}_{\mathrm{loc}}}\boldsymbol{F}^{t}\boldsymbol{D}^{\mathrm{e}}\boldsymbol{B}\,\mathrm{d}\Omega,\quad K_{\zeta\zeta}=-\frac{1}{A^{\mathrm{e}}}\int_{\Omega^{\mathrm{e}}_{\mathrm{loc}}}\boldsymbol{F}^{t}\boldsymbol{D}^{\mathrm{e}}\boldsymbol{G}\,\mathrm{d}\Omega-\tilde{\mathscr{H}}_{\delta},\end{aligned} \tag{4.18}$$

with $\boldsymbol{D}^{\mathrm{e}}$ representing the matrix form of $\boldsymbol{c}^{\mathrm{e}}$. Since ζ^{e} is discontinuous across elements, a condensed element stiffness matrix may be formed to yield

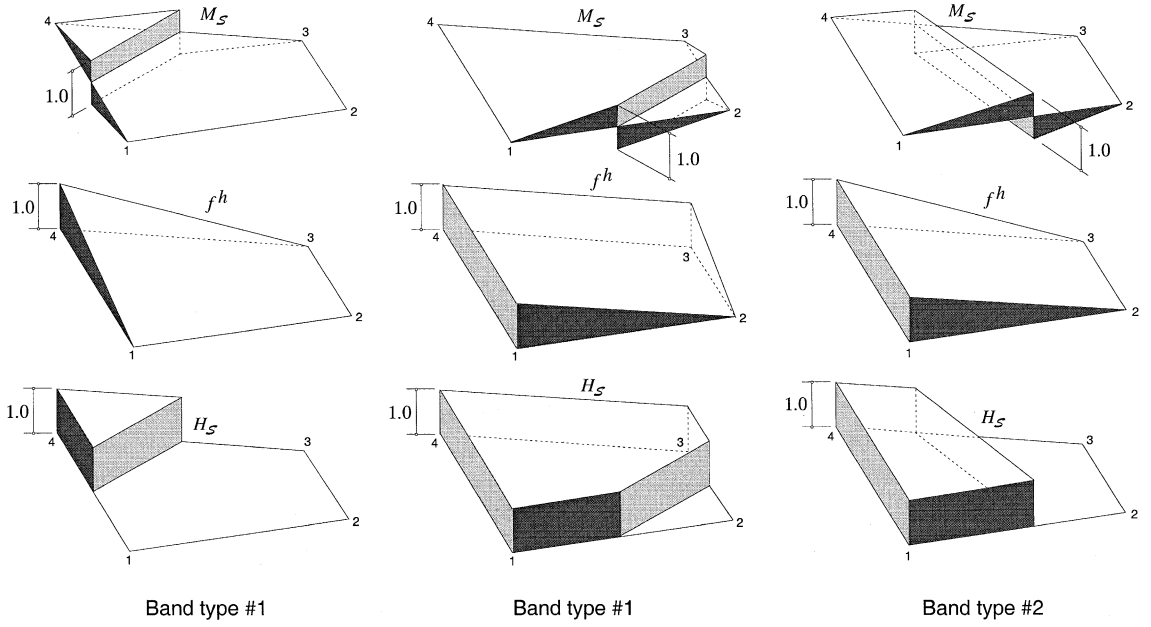

Fig. 7. Interpolation functions for band type #1 and band type #2.

$$\tilde{\boldsymbol{K}}^{\mathrm{e}} = \boldsymbol{K}^{\mathrm{e}}_{dd} - \boldsymbol{K}_{d\zeta} K^{-1}_{\zeta\zeta} \boldsymbol{K}_{\zeta d}. \tag{4.19}$$

Observe from (4.19) that for localized elements, the elastic stiffness matrix is effectively reduced by a "plastic" component arising from the slip along the surface of discontinuity.

Remark 6. The model presented above requires some special interpolation functions for localization analysis. The specific finite element for which the formulation will be tested is the four-noded bilinear quadrilateral element shown in Fig. 6. For this element, a band can form either by: (a) cutting one node of the element (band type #1); or (b) cutting two nodes (band type #2). In either case, the unit normal to the band is represented by the vector $\boldsymbol{n}$, while the slip direction is denoted by the vector $\boldsymbol{m}$. Fig. 7 shows the enhanced displacement interpolation functions describing the two band types. For band type #1, either one or three nodes bordering Ω^h_+ (on the surface $\mathscr{S}^h_+$) can be cut by the slip line. The latter case (three active nodes) can be incorporated quite easily into the algorithm pertaining to the former case (one active node) simply by changing the signs of the interpolation functions. Band type #1 shown in Fig. 7 requires an interpolation function $f^h = N_A$, where N_A is the standard (smooth) interpolation function associated with node $A \in \mathscr{S}^h_+$ of a typical bilinear quadrilateral element. Band type #2 requires an interpolation function $f^h = N_A + N_B$, where A and B are elements of the boundary $\mathscr{S}^h_+$.

5. Numerical examples

Plane strain compression problems are presented to demonstrate the degree of objectivity with respect to mesh refinement and insensitivity to mesh alignment of finite element solutions employing the Drucker–Prager model with displacement jumps. Objectivity with respect to mesh refinement is measured by the closeness of the force–displacement curves during softening, the enhanced solutions exhibiting mesh insensitivity compared to the standard solutions during softening. Insensitivity to mesh alignment is demonstrated by slip lines orienting sharply in the mesh without the element sides being aligned with the expected slip line orientation. We note that all meshes shown here are "unstructured" in the sense that no attempt is made to align element sides with an expected slip line orientation.

For numerical implementation, the localization condition (3.24) is rewritten herein in a slightly different form to read as follows:

$$\texttt{IF} \quad \left| \frac{3\sqrt{2}s_3}{\|\boldsymbol{s}\|} + (\beta + b) - \sqrt{\frac{2}{1-\nu}}(\beta - b) \right| \leqslant h^{\text{tol}} \quad \texttt{OR} \ \det(\boldsymbol{A}) \leqslant 0 \tag{5.1}$$

$\texttt{THEN}$ the element has localized.

The localization tolerance, h^{tol}, is an important parameter which must be chosen carefully. In general, h^{tol} may be small, but if it is too small, the slip line may not fully propagate through the mesh because the localization condition would be too strict for elements further along the slip line to localize, particularly with a coarse time-step size; as a result, localized softening would not be observed in the force-displacement plot. Depending on the time-step size, the criterion $\det(\boldsymbol{A}) \leqslant 0$ may be met rather than the first inequality in (5.1), but this first inequality will be met to the finest tolerance h^{tol} so desired if the time-step is refined enough. In the numerical examples, $h^{\text{tol}} = 1 \times 10^{-5}$ has been used.

The problem configuration is shown in Fig. 8. In this example, an irregular mesh composed of 63 elements and regular unstructured meshes with three levels of mesh refinement are used to analyze the problem: 75 element mesh, 300 element mesh, and 1200 element mesh (Fig. 9). Roller supports are placed on the boundaries in an attempt to provide a homogeneous state of stress prior to localization. Material properties are as follows: modulus of elasticity, $E = 2 \times 10^4$ kPa; Poisson's ratio, $\nu = 0.4$; $\alpha_0 = 17.14$ kPa; $\beta = 0.49487$ (calculated from (3.7) for $\overline{\phi} = 30°$ with a positive sign in the denominator); pre-localization plastic moduli for shear and volumetric components (see $(3.3)_2$), $H' = -50$ kPa and $K' = 0$; post-localization softening moduli, $H_\delta = -2000$ kPa/m and $K'_\delta = 0$ (given per meter because the delta function, $\delta_{\mathscr{S}}$, inherently has dimension of 1/length); and mobilized friction angle at post-localization, $\phi_{\mathscr{S}} = 30°$. Checks were routinely made to ensure that these moduli resulted in a bifurcated softening behavior (as opposed to continuum softening).

Note that the pre- and post-localization plastic moduli do not necessarily have to be the same (i.e. $H' \neq H_\delta$, $K' \neq K_\delta$) because at the onset of localization the solution bifurcates, and so the standard continuum plastic moduli have no meaning for the localized problem. As for the dilatation constant b, three values were tested: $b = \beta = 0.49487$ (associative, dilative plastic flow); $b = 0.3$ (non-associative, dilative plastic flow), and $b = 0$ (non-associative, deviatoric plastic flow). Note that the classical deviatoric Von Mises model is captured naturally by setting $b = \beta = 0$. In this case, and in other cases involving deviatoric plastic response, the $\overline{B}$-method [35] is employed to alleviate mesh locking.

Case 1 (*Associative*, *dilative plastic flow*). The deformed meshes (displacement magnification = 1.0) and load-displacement curves predicted by the standard and enhanced finite element solutions are shown in Figs. 9 and 10, respectively. For the enhanced solution the slip line is oriented at 30° to the compression axis, and the dilatancy angle ψ that $\boldsymbol{m}$ makes with the slip line is 31° (see Fig. 4). Since the state of stress prior to localization is homogeneous, localization is detected simultaneously in all elements. Consequently, there arise two possible shear band orientations and an infinite number of shear band positions. For presentation purposes one orientation of the slip line is chosen arbitrarily, as well as traced to the arbitrarily chosen positions shown in Fig. 9. The standard solutions predicted a persistent homogeneous state of stress beyond the bifurcation point; consequently the resulting load–displacement curves remain one on top of the other (Fig. 10), although the accelerated softening response is not captured by the standard solutions. On

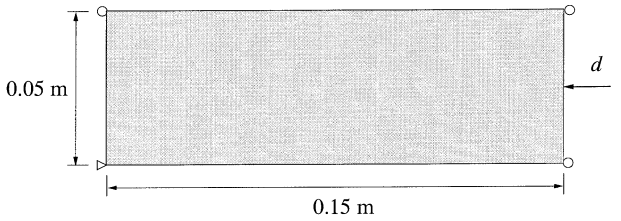

Fig. 8. Plane strain compression problem with prescribed displacement, d.

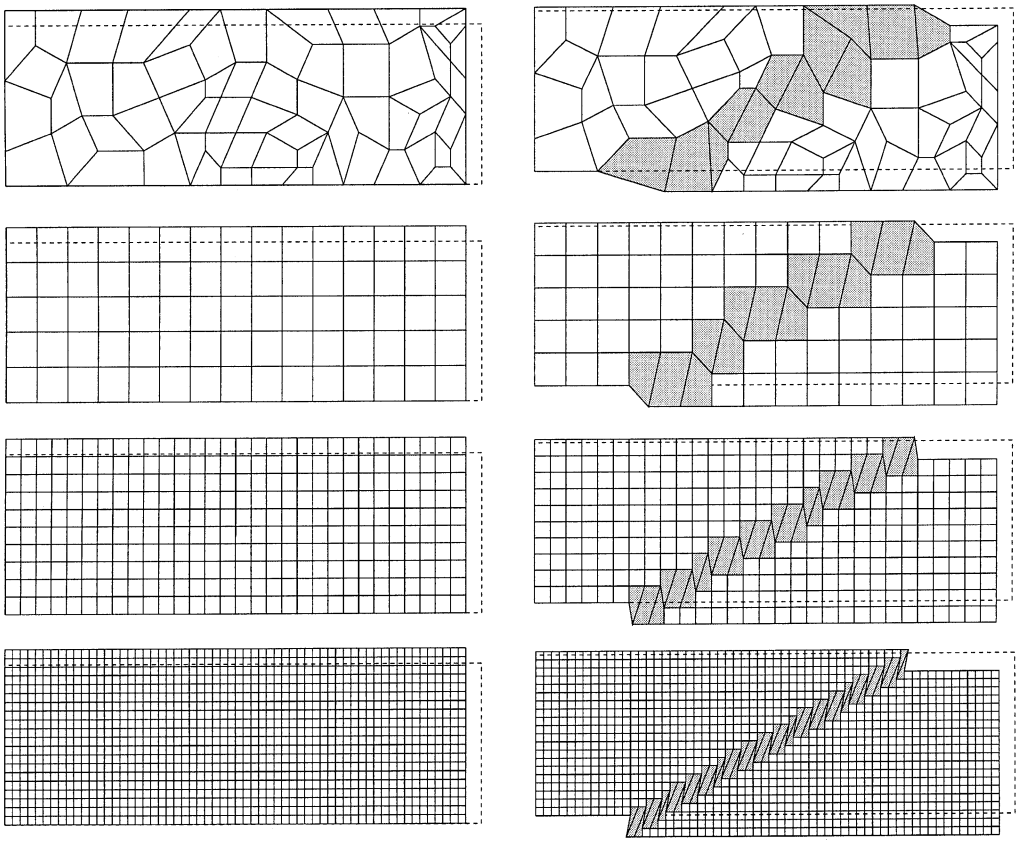

Fig. 9. Plane strain compression problem: associative, dilative plastic flow ($\beta = b = 0.49487$).

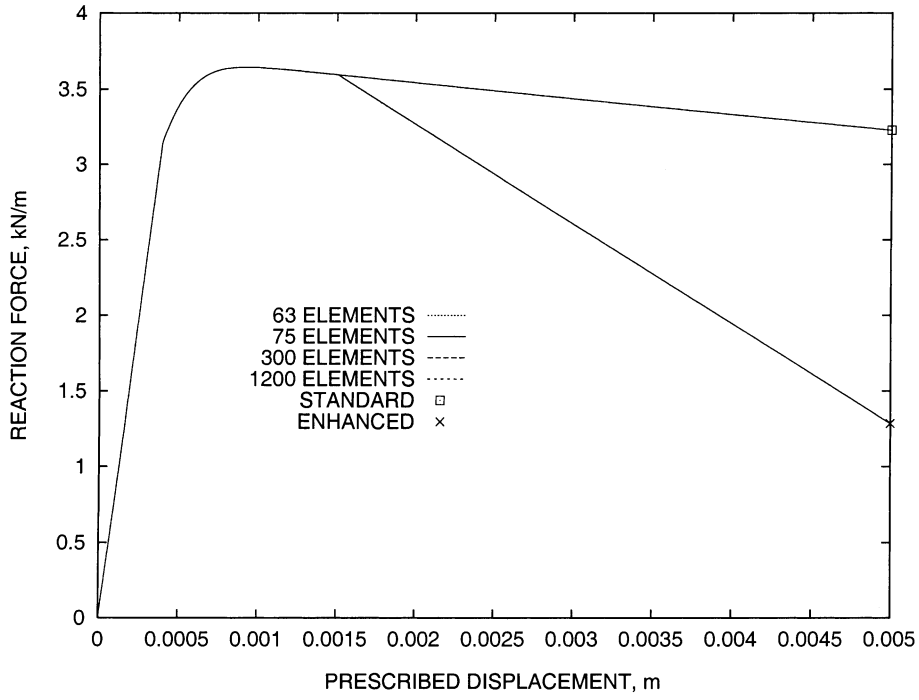

Fig. 10. Plane strain compression problem: associative, dilative plastic flow ($\beta = b = 0.49487$).

the other hand, the enhanced solutions also plot one on top of the other before and after localization, as well as clearly show capability to capture the accelerated softening response after localization. The post-localization responses predicted by the enhanced solutions are identical to machine precision.

Case 2 (*Non-associative*, *dilative plastic flow*). The deformed meshes and load–displacement curves predicted by the standard and enhanced finite element solutions are shown in Figs. 11 and 12, respectively. For the enhanced solution, the slip line is oriented at 35° to the compression axis, and the dilatancy angle ψ that $\boldsymbol{m}$ makes with the slip line is 19°. The standard solutions with 63 and 75 elements predicted persistent homogeneous states of stress after localization (also evident by the standard deformed meshes remaining rectangular in Fig. 11), whereas the 300 and 1200 element meshes demonstrate mesh dependence for the standard plasticity solution (also evident by the corresponding standard deformed meshes deforming non-homogeneously as shown in Fig. 11). It is common for non-associative softening plasticity that localization is detected *before* the standard solution curves are seen to deviate from one another, as shown in Fig. 12 as well as in later figures. On the other hand, the enhanced solutions remain absolutely mesh-insensitive as affirmed by the load–displacement curves remaining one on top of the other in Fig. 12. Note that the 1200 element standard solution curve is shown in Fig. 12 (as well as in Figs. 14 and 16) only to the point where it could not be converged further.

Case 3 (*Non-associative*, *dilative plastic flow with weak element*). In Fig. 13 a weak element is introduced (α_0 is reduced by 1%) at the locations specified by the blackened elements. This perturbation created a non-homogeneous stress field. The deformed meshes and load–displacement curves predicted by the standard and enhanced finite element solutions are shown in Figs. 13 and 14, respectively. As expected, the standard solutions demonstrate mesh-dependence. Also, the enhanced solutions are not exactly one on top of the other as demonstrated in Fig. 14 because the stress state is not uniform (which means the stresses at

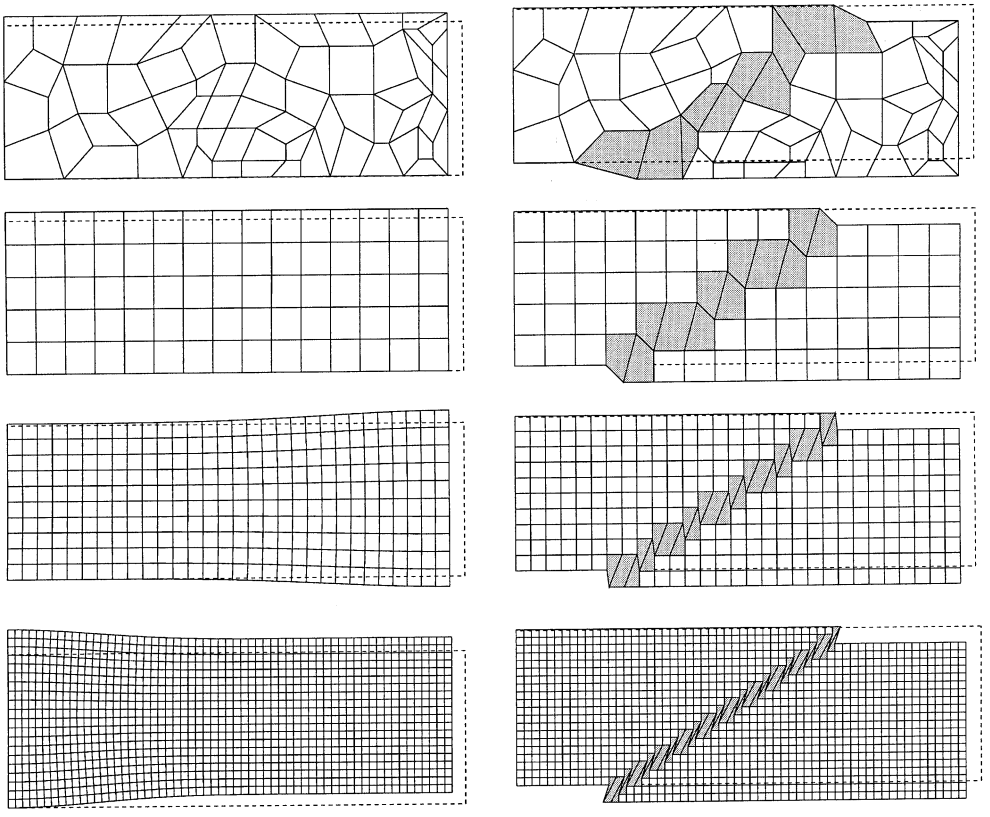

Fig. 11. Plane strain compression problem: non-associative, dilative plastic flow ($\beta = 0.49487,\ b = 0.3$).

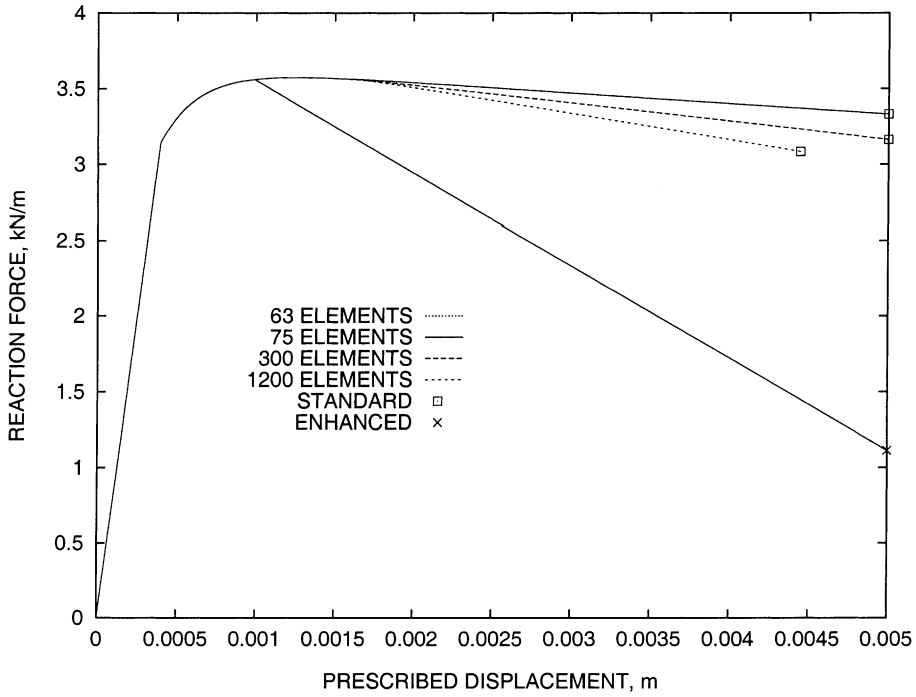

Fig. 12. Plane strain compression problem: non-associative, dilative plastic flow ($\beta = 0.49487,\ b = 0.3$).

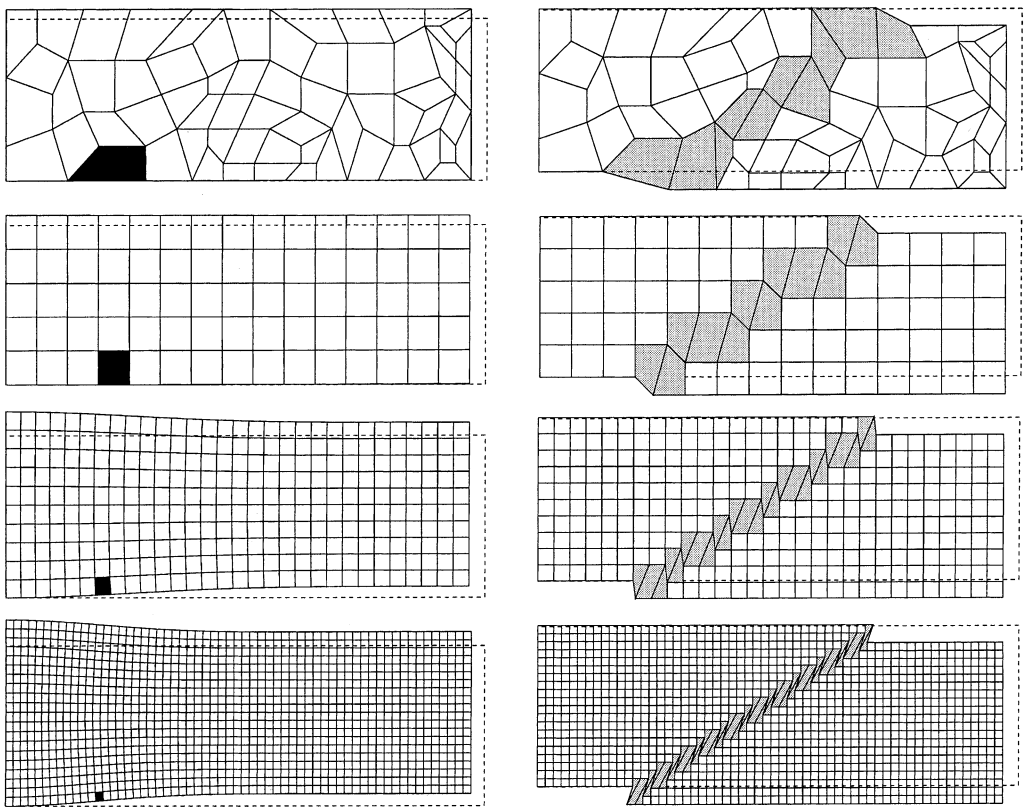

Fig. 13. Plane strain compression problem with weak element: non-associative, dilative plastic flow ($\beta = 0.49487,\ b = 0.3$). Location of weakened elements indicated by blackened elements on the deformed meshes resulting from the standard finite element solution.

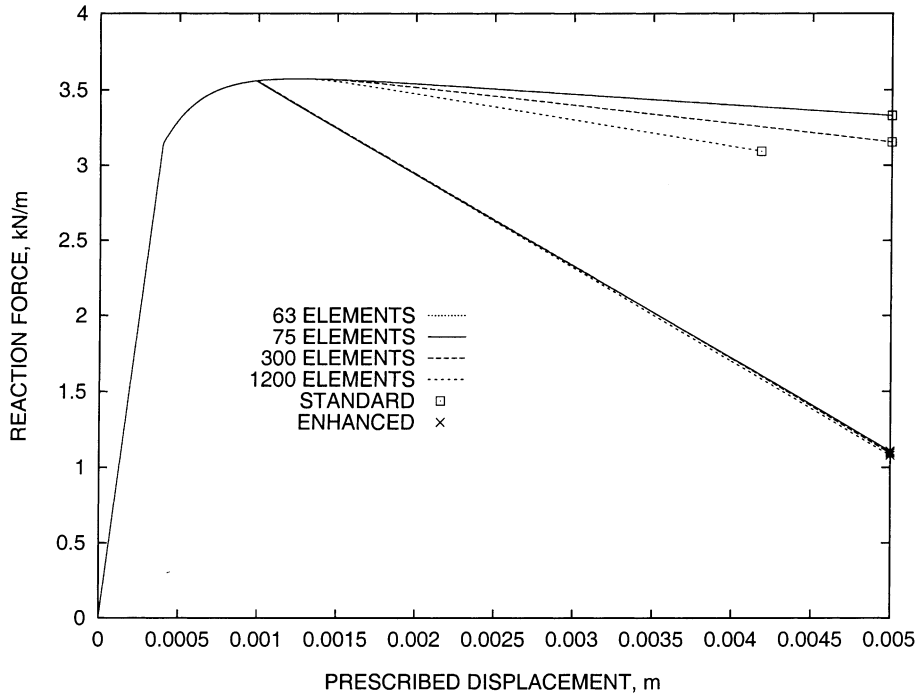

Fig. 14. Plane strain compression problem with weak element: non-associative, dilative plastic flow ($\beta = 0.49487,\ b = 0.3$).

pre-localization are not identical to machine precision due to the finite element approximations, and so the onset of localization does not occur simultaneously in all elements). However, the curves are close enough to call the enhanced solution mesh-independent.

Case 4 (*Non-associative, deviatoric plastic flow*). Figs. 15 and 16 show mesh-dependence for each standard solution but identical load–displacement curves for the enhanced solutions (no weak element is used). For this case, the slip line is oriented at 39° to the compression axis, whereby the angle ψ that $\boldsymbol{m}$ makes with the slip line is 2°. Note that $\psi \neq 0$ even if $b = 0$ because $\beta \neq 0$. This means that some small dilatancy is predicted at the onset of localization even if the dilation angle of the intact material is zero due to frictional effects. The enhanced solution curves are seen to bifurcate right at the onset of plastic flow.

Remark 7. Note that in Figs. 11 and 15 there are no weak elements or other inhomogeneities to trigger localized deformation in the standard solution, but due to the ill-posed governing partial differential equation it is possible that localization could be triggered even by the predictor–corrector approach to numerically integrating the rate-constitutive equations. For the record, a standard fully implicit backward integration is performed in all of the analyses, and the numerical solutions all converged to an absolute tolerance of 1×10^{-10} on the Euclidean norm of the vector residual in (4.15) and the scalar residual in (4.16).

Finally, contours of octahedral shear strains generated by the enhanced solutions for Cases 2 and 4 are compared in Fig. 17. Here, the strains were evaluated at the Gauss points based on the computed total nodal displacements, and hence represent the conforming part of the total strain tensor, $\mathrm{conf}(\boldsymbol{\epsilon}_{\mathrm{e}}^h) = \mathrm{sym}(\nabla \overline{\boldsymbol{u}}^h)$, see (4.9a). The enhanced part just outside of the shear band is obtained from (4.9b) as $-\zeta^{\mathrm{e}}\mathrm{sym}(\nabla f_{\mathrm{e}}^h \otimes \boldsymbol{m})$, which, when added to the conforming part, produces approximately a uniform strain field (not shown since it is trivially uniform). Recall that the contribution of the enhanced part is condensed statically on the element level to get the total solution. Fig. 17 shows that the effect of dilatancy is to slightly intensify the conforming octahedral shear strains, Fig. 17(a), as compared to the deviatoric case, Fig. 17(b). Furthermore, refining the mesh results in more intense conforming octahedral shear strains near the band,

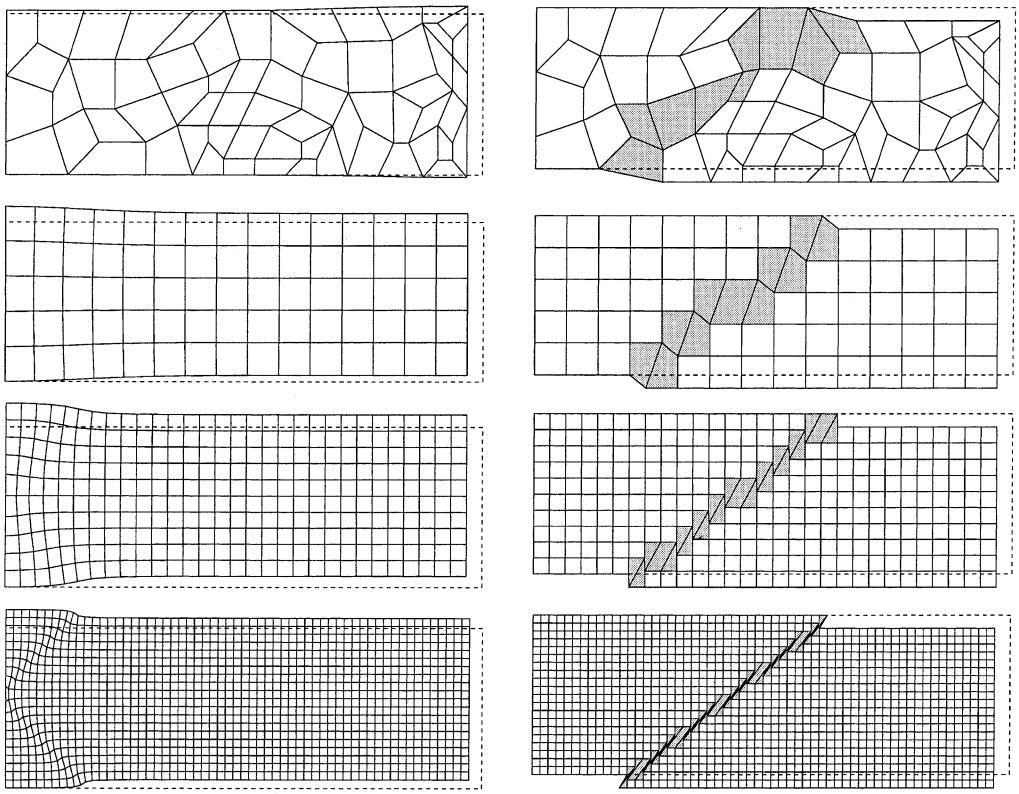

Fig. 15. Plane strain compression problem: non-associative, deviatoric plastic flow ($\beta = 0.49487,\ b = 0$). Bilinear quadrilaterals with $\overline{B}$.

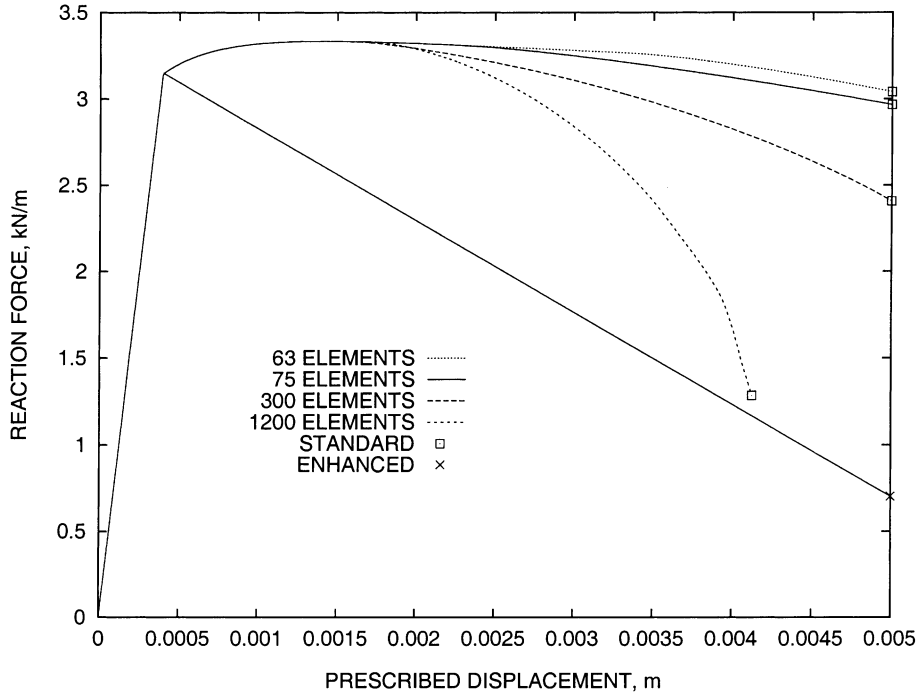

Fig. 16. Plane strain compression problem: non-associative, deviatoric plastic flow ($\beta = 0.49487,\ b = 0$).

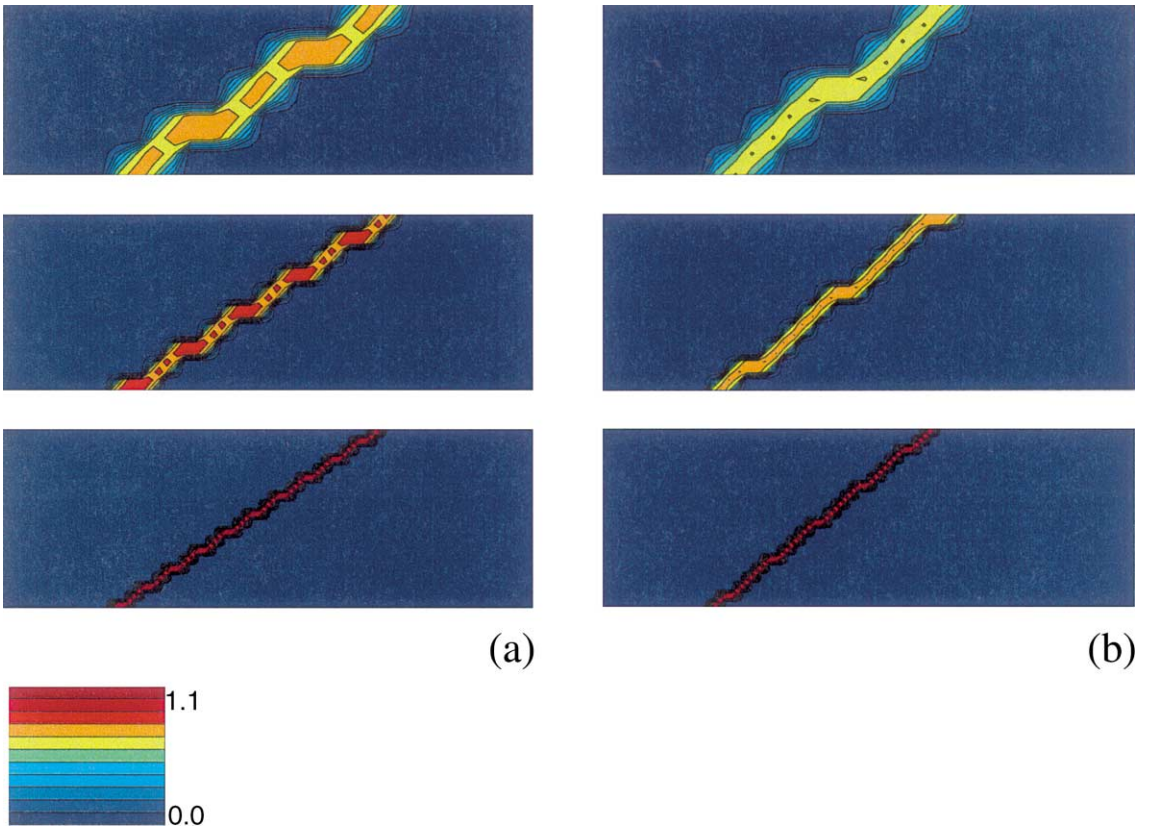

Fig. 17. Conforming octahedral shear strains from enhanced finite element solutions: (a) non-associative, dilative; (b) non-associative, deviatoric. From top to bottom: 75 element mesh; 300 element mesh; 1200 element mesh.

but concentrated over a narrower zone. Of course, the total strain field in all cases is singular on $\mathscr{S}$ due to an additional term associated with $\delta_{\mathscr{S}}$, see (4.9b). Fig. 17 adds context to the mesh-insensitivity of the enhanced finite element solution because, no matter how mesh-dependent the conforming part is, the total strain field just outside the shear band remains essentially unaffected by the mesh refinement.

6. Summary and conclusion

We have presented a mathematical model for analyzing strain localization in frictional solids exhibiting displacement jumps. Precise conditions for the appearance of slip lines are outlined for a rate-independent, strain-softening Drucker–Prager model. The formulation is cast within the framework of finite element analysis employing the assumed enhanced strain method. Numerical examples involving plane strain compression at varying levels of non-associativity, with and without a weak element, have demonstrated objectivity with respect to mesh refinement and insensitivity to mesh alignment of the enhanced finite element solutions. Results presented in this paper have significant impact in modeling many complex mechanical behavior of soils and rocks experiencing highly localized patterns of deformation, eventually leading to displacement discontinuities.

Acknowledgements

The work presented in this paper was supported by the G3S Division of the National Science Foundation through Grant No. CMS97-00426 under the directorship of Dr. Priscilla P. Nelson. We acknowl-

edge the use of the Sun Sparc20's in the Advanced Computing Environment (ACE) laboratory, and the Sun Ultra2's in the John A. Blume Earthquake Engineering Center, both part of the Civil and Environmental Engineering Department at Stanford University. We thank Dr. Krishna Garikipati of Stanford University for invaluable discussions regarding some important aspects of the strong discontinuity model.

References

[1] J.C. Simo, J. Oliver, F. Armero, An analysis of strong discontinuities induced by strain-softening in rate-independent inelastic solids, Comput. Mech. 12 (1993) 277–296.
[2] T.W. Lambe, R.V. Whitman, Soil Mechanics, Wiley, New York, 1969.
[3] M.J. Hvorslev, Physical components of the shear strength of saturated clays, in: Research Conference on Shear Strength of Cohesive Soils, ASCE, June 1960, pp. 169–273.
[4] K.H. Roscoe, The influence of strains in soil mechanics, 10th Rankine Lecture, Géotechnique 20 (2) (1970) 129–170.
[5] G. Scarpelli, D.M. Woods, Experimental observations of shear band patterns in direct shear tests, in: Proceedings of the IUTAM Conference on Deformation and Failure of Granular Materials, Delft, Balkema Publ., Rotterdam, 1982, pp. 473–484.
[6] C.A. Coulomb, Essai sur une application des règles de Maximus et Minimis à quelques Problèmes de Statique, relatifs à l' Architecture, in: Mémoires de Mathématique et de Physique, vol. 7, Présentés a l' Académie Royale des Sciences, par divers Savans, et lûs dans ses Assemblées, Paris, 1776, pp. 343–382.
[7] W.J.M. Rankine, On the stability of loose earth, Philos. Trans. Roy. Soc. London 147 (1) (1857) 9–27.
[8] K. Terzaghi, Theoretical Soil Mechanics, Wiley, New York, 1943.
[9] G.G. Meyerhof, The ultimate bearing capacity of foundations, Géotechnique 2 (1951) 301–332.
[10] A.W. Bishop, The use of the slip circle in the stability analysis of earth slopes, Géotechnique 5 (1955) 7–17.
[11] N. Janbu, L. Bjerrum, B. Kjaernsli, Veiledning ved losing av fundamenteringsoppgaver, vol. 16, Norwegian Geotechnical Institute Publications, Oslo, 1956.
[12] W. Johnson, Henri Tresca as the originator of adiabatic heat lines, Int. J. Mech. Sci. (1987) 301–310.
[13] F. Armero, K. Garikipati, Recent advances in the analysis and numerical simulation of strain localization in inelastic solids, in: D.R.J. Owen, E. Oñate, E. Hinton (Eds.), Proceedings of Computational Plasticity IV, CIMNE, Barcelona, Spain, 1995, pp. 547–561.
[14] K.R. Garikipati, On strong discontinuities in inelastic solids and their numerical simulation, Ph.D. thesis, Stanford University, Stanford, California, 1996.
[15] R. Larsson, K. Runesson, S. Sture, Embedded localization band in undrained soil based on regularized strong discontinuity theory and FE analysis, Int. J. Solids Struct. 33 (1996) 3081–3101.
[16] R. Larsson, K. Runesson, N.S. Ottosen, Discontinuous displacement approximation for capturing plastic localization, Int. J. Numer. Methods Engrg. 36 (1993) 2087–2105.
[17] K. Runesson, D. Peric, S. Sture, Discontinuous bifurcations of elastic–plastic solutions at plane stress and plane strain, Int. J. Plasticity 7 (1991) 99–121.
[18] J.C. Simo, J. Oliver, A new approach to the analysis and simulation of strain softening in solids, in: Z.P. Bazant, Z. Bittnar, M. Jirásek, J. Mazars (Eds.), E&FN Spon, 2–6 Boundary Row, London, 1994, pp. 25–39 (Chapter 3: Fracture and Damage in Quasibrittle Structures).
[19] J.C. Simo, M.S. Rifai, A class of mixed assumed strain methods and the method of incompatible modes, Int. J. Numer. Methods Engrg. 29 (1990) 1595–1638.
[20] M. Ortiz, Y. Leroy, A. Needleman, A finite element method for localized failure analysis, Comput. Methods Appl. Mech. Engrg. 61 (1987) 189–214.
[21] Y. Leroy, M. Ortiz, Finite element analysis of transient strain localization phenomena in frictional solids, Int. J. Numer. Methods Engrg. 14 (1990) 93–124.
[22] B. Loret, J.H. Prevost, Dynamic strain localization in elasto-(visco-)plastic solids, Part 1. General formulation and one-dimensional examples, Comput. Methods Appl. Mech. Engrg. 83 (1990) 247–273.
[23] J.H. Prevost, B. Loret, Dynamic strain localization in elasto-(visco-)plastic solids, Part 2. Plane strain examples, Comput. Methods Appl. Mech. Engrg. 83 (1990) 275–294.
[24] N. Triantafyllidis, E.C. Aifantis, A gradient approach to localization of deformation. I: Hyperelastic materials, J. Elasticity 16 (1986) 225–237.
[25] R. de Borst, L.J. Sluys, Localisation in a Cosserat continuum under static and dynamic loading conditions, Comput. Methods Appl. Mech. Engrg. 90 (1991) 805–827.
[26] H. Matthies, G. Strang, E. Christiansen, The saddle point of a differential program, in: R. Glowinski, E.Y. Rodin. O.C. Zienkiewicz (Eds.), Energy Methods in Finite Element Analysis, Wiley, Chichester, 1979, pp. 309–318 (Chapter 17).
[27] P.-M. Suquet, Existence and regularity of solutions for plasticity problems, in: S. Nemat-Nasser (Ed.), Variational Methods in the Mechanics of Solids, Pergamon, Oxford, 1980, pp. 304–309.
[28] I. Stakgold, Green's Functions and Boundary Value Problems, Second ed., Wiley, New York, 1998.
[29] J. Oliver, M. Cervera, O. Manzoli, On the use of J_2 plasticity models for the simulation of 2D strong discontinuities in solids, in: D.R.J. Owen, E. Hinton (Eds.), Computational Plaicity Fundamentals and Applications, CIMNE, Barcelona, 1997, pp. 38–55.
[30] R. Butterfield, A natural compression law for soils, Géotechnique 29 (1979) 469–480.

[31] R.I. Borja, C. Tamagnini, A. Amorosi, Coupling plasticity and energy-conserving elasticity models for clays, J. Geotech. Geoenvironmental Engrg., ASCE 123 (10) (1997) 948–957.
[32] R.I. Borja, C. Tamagnini, Cam-clay plasticity, Part III: Extension of the infinitesimal model to include finite strains, Comput. Methods Appl. Mech Engrg. 155 (1998) 73–95.
[33] D.R.J. Owen, E. Hinton, Finite Elements in Plasticity: Theory and Practice, Pineridge Press, UK, 1980.
[34] J.E. Marsden, T.J.R. Hughes, Mathematical Foundations of Elasticity, Prentice-Hall, Englewood Cliffs, NJ, 1983.
[35] T.J.R. Hughes, Generalization of selective integration procedures to anisotropic and nonlinear media, Int. J. Numer. Methods Engrg. 15 (1980) 1413–1418.